Calcium sparks enhance the tissue fluidity within epithelial layers and promote apical extrusion of transformed cells

AUTHOR(S):

Kuromiya, Keisuke; Aoki, Kana; Ishibashi, Kojiro; Yotabun, Moe; Sekai, Miho; Tanimura, Nobuyuki; Iijima, Sayuri; ... Sugimura, Kaoru; Hino, Naoya; Fujita, Yasuyuki

CITATION:

Kuromiya, Keisuke ...[et al]. Calcium sparks enhance the tissue fluidity within epithelial layers and promote apical extrusion of transformed cells. Cell Reports 2022, 40(2): 111078.

ISSUE DATE:

2022-07-12

URL:

http://hdl.handle.net/2433/284956

Article

Cell Reports

Calcium sparks enhance the tissue fluidity within epithelial layers and promote apical extrusion of transformed cells

Graphical abstract

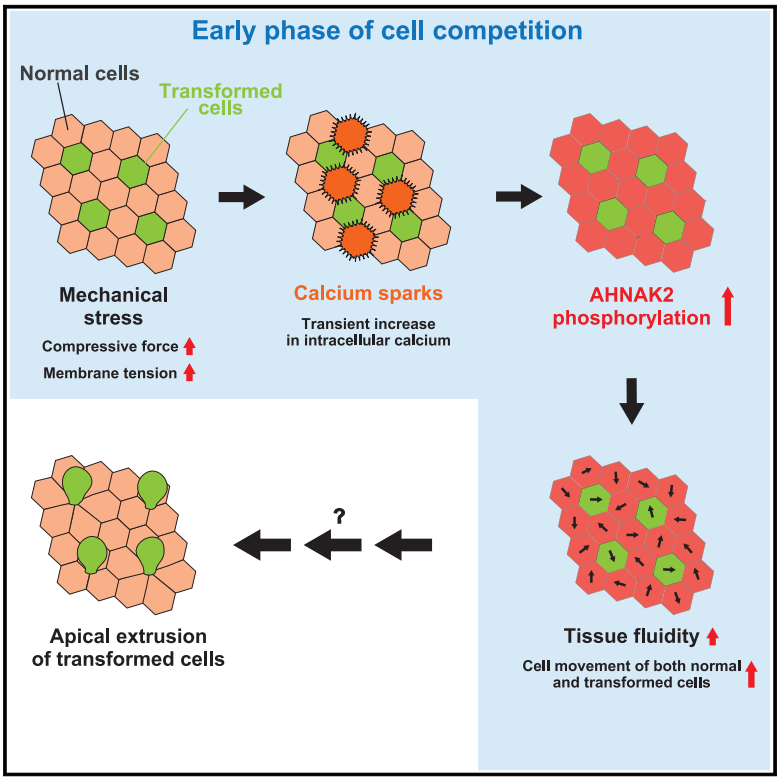

Highlights

- Phosphorylation of AHNAK2 is elevated in normal cells neighboring transformed cells
- TRPC1-mediated calcium sparks in normal cells mediate the AHNAK2 phosphorylation
- Calcium sparks promote tissue fluidity and apical extrusion of transformed cells
- Comparable calcium sparks regulate apical extrusion in cultured cells and zebrafish

Authors

Keisuke Kuromiya, Kana Aoki, Kojiro Ishibashi, ..., Kaoru Sugimura, Naoya Hino, Yasuyuki Fujita

Correspondence

fujita@monc.med.kyoto-u.ac.jp

In brief

Kuromiya et al. use mammalian cell culture and zebrafish systems to show that calcium sparks frequently occur in normal epithelial cells neighboring RasV12-transformed cells at the early phase of cell competition. Calcium sparks then promote epithelial tissue fluidity and apical extrusion of transformed cells through the phosphorylation of AHNAK2.

Kuromiya et al., 2022, Cell Reports *40*, 111078
July 12, 2022
https://doi.org/10.1016/j.celrep.2022.111078

CellPress

Cell Reports

CellPress OPEN ACCESS

Article

Calcium sparks enhance the tissue fluidity within epithelial layers and promote apical extrusion of transformed cells

Keisuke Kuromiya,[1,2,13] Kana Aoki,[3,13] Kojiro Ishibashi,[2,13] Moe Yotabun,[1] Miho Sekai,[1,4] Nobuyuki Tanimura,[1,2] Sayuri Iijima,[2] Susumu Ishikawa,[2] Tomoko Kamasaki,[2] Yuki Akieda,[3] Tohru Ishitani,[3] Takashi Hayashi,[5] Satoshi Toda,[6] Koji Yokoyama,[7] Chol Gyu Lee,[7] Ippei Usami,[7] Haruki Inoue,[7] Ichigaku Takigawa,[8,9] Estelle Gauquelin,[10] Kaoru Sugimura,[10,11] Naoya Hino,[12] and Yasuyuki Fujita[1,2,14,*]

[1]Department of Molecular Oncology, Graduate School of Medicine, Kyoto University, Kyoto, Japan
[2]Division of Molecular Oncology, Institute for Genetic Medicine, Hokkaido University Graduate School of Chemical Sciences and Engineering, Sapporo, Japan
[3]Division of Cellular and Molecular Biology, Department of Homeostatic Regulation, Research Institute for Microbial Diseases, Osaka University, Osaka, Japan
[4]KAN Research Institute, Kobe, Japan
[5]Department of Lead Discovery Research, New Drug Research Division, Otsuka Pharmaceutical, Tokushima, Japan
[6]WPI Nano Life Science Institute, Kanazawa University, Kanazawa, Japan
[7]HACARUS, Kyoto, Japan
[8]RIKEN Center for Advanced Intelligence Project, Kyoto, Japan
[9]Institute for Chemical Reaction Design and Discovery, Hokkaido University, Sapporo, Japan
[10]Department of Biological Sciences, Graduate School of Science, The University of Tokyo, Tokyo, Japan
[11]Institute for Integrated Cell-Material Sciences (WPI-iCeMS), Kyoto University, Kyoto, Japan
[12]Research Center for Dynamic Living Systems, Graduate School of Biostudies, Kyoto University, Kyoto, Japan
[13]These authors contributed equally
[14]Lead contact
*Correspondence: fujita@monc.med.kyoto-u.ac.jp
https://doi.org/10.1016/j.celrep.2022.111078

SUMMARY

In vertebrates, newly emerging transformed cells are often apically extruded from epithelial layers through cell competition with surrounding normal epithelial cells. However, the underlying molecular mechanism remains elusive. Here, using phospho-SILAC screening, we show that phosphorylation of AHNAK2 is elevated in normal cells neighboring RasV12 cells soon after the induction of RasV12 expression, which is mediated by calcium-dependent protein kinase C. In addition, transient upsurges of intracellular calcium, which we call calcium sparks, frequently occur in normal cells neighboring RasV12 cells, which are mediated by mechanosensitive calcium channel TRPC1 upon membrane stretching. Calcium sparks then enhance cell movements of both normal and RasV12 cells through phosphorylation of AHNAK2 and promote apical extrusion. Moreover, comparable calcium sparks positively regulate apical extrusion of RasV12-transformed cells in zebrafish larvae as well. Hence, calcium sparks play a crucial role in the elimination of transformed cells at the early phase of cell competition.

INTRODUCTION

Throughout the lifespan of multicellular organisms, oncogenic transformation can occur in single cells within epithelial layers. Previous studies have demonstrated that the newly emerging transformed cells are often eliminated from epithelial layers via cell competition with the surrounding normal epithelial cells. Cell competition is a process by which cells with different properties compete with one another for survival and space; loser cells are eliminated from the cellular society, while winner cells proliferate and fill the vacant spaces (Amoyel and Bach, 2014; Baker, 2020; Bowling et al., 2019; Diaz-Diaz and Torres, 2019; Johnston, 2009; Levayer, 2020; Madan et al., 2018; Maruyama and Fujita, 2017; Morata and Calleja, 2020; Vishwakarma and Piddini, 2020). Cell competition was originally found in *Drosophila* (Morata and Ripoll, 1975), but it also occurs in higher organisms such as zebrafish and mice (Maruyama and Fujita, 2017). Cell death-independent extrusion of transformed cells is one of the phenotypes of loser cells among a variety of cell competition phenomena. For example, in mammalian cell culture, zebrafish, and mouse model systems, when RasV12-, Src-, or ErbB2-transformed cells are surrounded by normal epithelial cells, transformed cells are apically extruded from the epithelial monolayer through cell competition with the

surrounding normal cells (Hogan et al., 2009; Kajita et al., 2010; Kon et al., 2017; Leung and Brugge, 2012; Sasaki et al., 2018; Takeuchi et al., 2020; Wu et al., 2014). Cell competition is, in general, triggered by the intercellular recognition between winner and loser cells. After they recognize the differences between them, various non-cell-autonomous changes are induced in both winner and loser cells, eventually leading to the elimination of loser cells. Recent studies have revealed that multiple non-cell-autonomous changes occur at the late stage of the cell competition between normal and RasV12 cells. For instance, cytoskeletal proteins filamin and vimentin accumulate in the surrounding normal cells at the interface with transformed cells, which generate physical forces for apical extrusion (Kajita et al., 2014). In turn, in transformed cells surrounded by normal cells, Warburg effect-like metabolic changes occur, which positively regulate apical extrusion (Kon et al., 2017). However, what happens at the earlier stage of cell competition when normal and transformed cells start recognizing their differences from each other remains elusive.

It has been reported that the two modes of calcium signals play crucial roles in intercellular communications: calcium wave and calcium spike (or spark) (Markova and Lenne, 2012). A previous study has demonstrated that calcium wave is involved in the later stage of cell competition (Takeuchi et al., 2020). Just before the completion of apical extrusion, calcium wave propagates from extruding transformed cells across the surrounding normal cells. The surrounding cells that have received calcium wave show the polarized movement toward extruding cells, thereby promoting the process of apical extrusion. However, it remains unknown whether calcium signals also play a certain role at the earlier stage of cell competition.

In this study, we demonstrate that at the early phase of cell competition, another calcium-mediated phenomenon, calcium spark, enhances cell movements within the epithelial layer and promotes the apical elimination of transformed cells.

RESULTS

Phosphorylation of AHNAK2 is enhanced during the early phase of cell competition between normal and RasV12- or Src-transformed cells

To investigate cell competition between normal and transformed cells, we have established Madin-Darby canine kidney (MDCK) epithelial cells that stably express GFP-RasV12 or GFP-cSrcY527F in a tetracycline-inducible manner (Hogan et al., 2009; Ohoka et al., 2015). In previous studies, using these cell lines, we have demonstrated that when RasV12- or Src-transformed cells are surrounded by normal epithelial cells, the transformed cells are apically extruded from the epithelial monolayer via cell competition between normal and transformed cells (Hogan et al., 2009; Ohoka et al., 2015). Various non-cell-autonomous changes, such as accumulation of filamin or Warburg effect-like metabolic changes, are observed after 16 h of the induction of RasV12 or cSrcY527F expression by tetracycline, followed by apical extrusion that occurs after 18–24 h of the tetracycline addition (Figure S6A) (Kajita et al., 2014; Kon et al., 2017). To identify crucial regulators for the earlier phase of cell competition, we performed stable isotope labeling with amino acids in cell culture (SILAC)-based quantitative mass spectrometric analyses targeting phosphorylated peptides (Olsen et al., 2006) after 6 or 10 h of tetracycline treatment. Two types of isotope-labeled lysine and arginine were used for cell labeling: medium (Lys4, Arg6) and heavy (Lys8, Arg10). Medium-labeled normal MDCK and RasV12- or Src-transformed cells were monocultured separately, whereas heavy-labeled MDCK and RasV12- or Src-transformed MDCK cells were mix cultured at 1:1 (Figure S1A). After 6 or 10 h of tetracycline treatment, cell lysates were collected from each condition, and those from the monoculture of normal and transformed cells were combined, followed by trypsin digestion and enrichment of phosphopeptides with titanium dioxide beads. Thereafter, the amounts of medium- and heavy-labeled peptides were compared by liquid chromatography-tandem mass spectrometry (LC-MS/MS). The relative protein abundance ratio (mix culture/monoculture) was calculated based on the signal intensities of mass spectra for heavy-labeled peptides relative to those for medium-labeled peptides, which represents the difference between the two culture states. We identified a number of proteins for which phosphorylation was elevated in mix culture compared with monoculture (Figures S1B and S1C; Table S1). Among the identified proteins, phosphorylation of AHNAK2 was upregulated under all four conditions (Ras 6 h, Ras 10 h, Src 6 h, and Src 10 h) (Figures S1B and S1C; Table S1). Five AHNAK2 peptides were detected in the analysis, but the increased SILAC ratio (mix culture/monoculture) was found only in three peptides that include a phosphorylated serine residue (MP[pS]FGASTPSK) (Figures S1D and S1E). Canine AHNAK2 has a large central region encompassing 6 highly analogous repeat domains with 168 or 182 amino acid residues, each of which contains the phosphorylation site identified by the phospho-SILAC screening (Figures S1F and S1G). To date, no reports have demonstrated the phosphorylation of AHNAK2.

Phosphorylation of AHNAK2 is elevated in normal cells mix cultured with RasV12- or Src-transformed cells

To examine the phosphorylation of AHNAK2, we generated both anti-AHNAK2 and anti-phospho-AHNAK2-specific antibodies. By immunofluorescence, anti-AHNAK2 antibody recognized both wild-type (WT) and non-phosphorylatable (SA mutant; serine was substituted for alanine in all six repeat domains) AHNAK2, whereas anti-phospho-AHNAK2 antibody recognized WT, but not SA mutant, of AHNAK2 (Figure S2A). Using these antibodies, we then analyzed the phosphorylation status of AHNAK2 at 6 h after the induction of RasV12 expression. By immunofluorescence with anti-phospho-AHNAK2 antibody, we showed that the level of AHNAK2 phosphorylation remained low under the monoculture condition of normal or RasV12-transformed cells (Figures 1A and 1B). In contrast, the phosphorylation of AHNAK2 was substantially elevated in normal cells, but not in RasV12 cells, under the mix culture condition (1:1) (Figures 1A and 1B). Increased phosphorylation was observed in normal cells directly contacting RasV12 cells as well as normal cells at the second row from RasV12 cells (Figures 1A and 1B). Upregulation of AHNAK2 phosphorylation was also observed under the 10:1 mix culture condition of normal and RasV12 cells (Figure S2B). By immunofluorescence with anti-AHNAK2

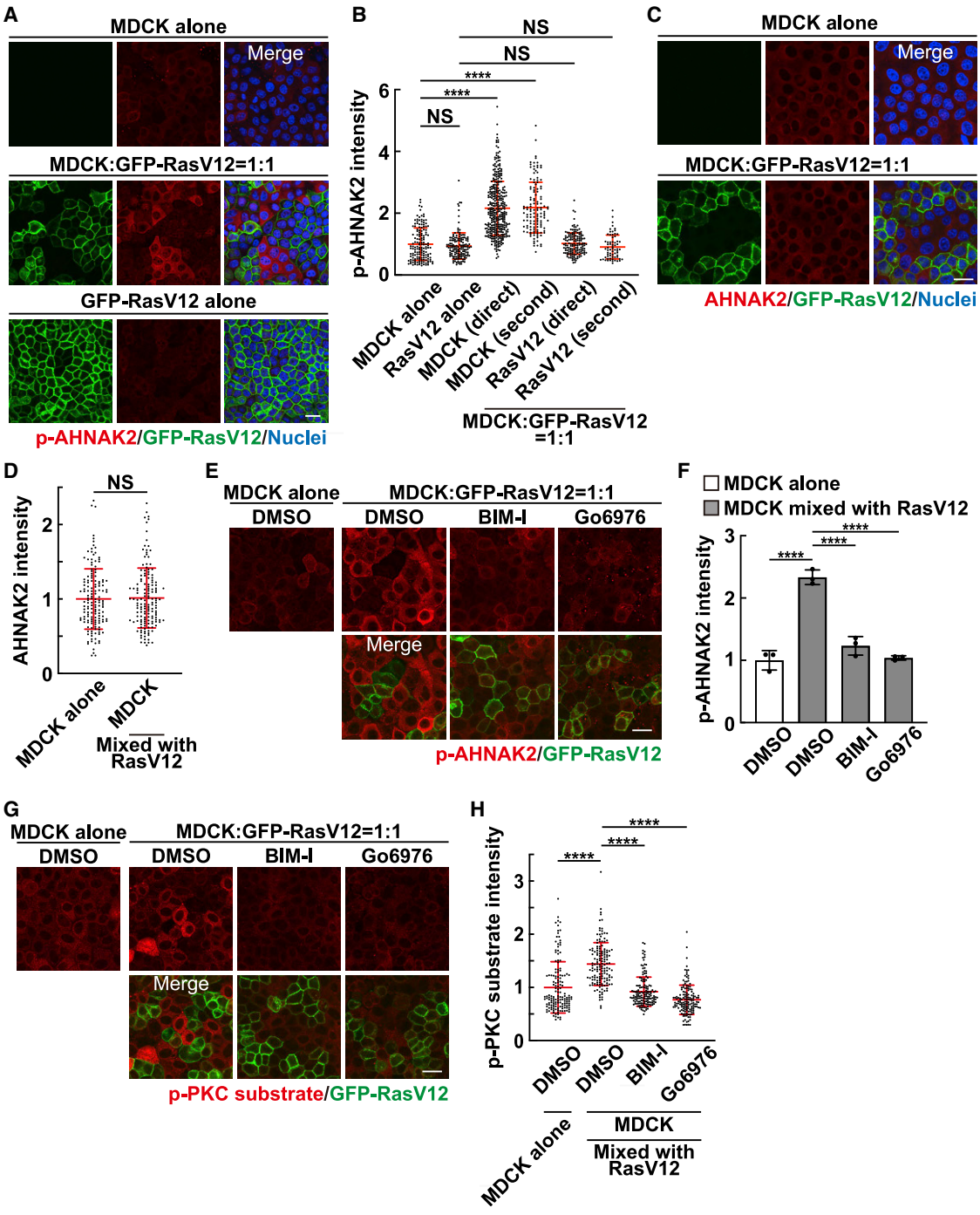

Figure 1. Phosphorylation of AHNAK2 is up-regulated in normal cells mix cultured with RasV12-transformed cells

(A and B) Phosphorylation of AHNAK2 in monoculture or mix culture of normal and RasV12-transformed cells. (A) Immunofluorescence images of p-AHNAK2. (B) Quantification of fluorescence intensity of p-AHNAK2; "direct" or "second" indicates cells directly contacting or in the second row. Values are expressed as a ratio relative to the average of MDCK alone. Cumulative data from 3 independent experiments are shown as means ± SDs. ****$p < 0.0001$ and NS, not significant (1-way ANOVA with Tukey's test); n = 150, 150, 355, 127, 150, and 67 cells.

(C and D) The level of AHNAK2 proteins in monoculture of normal cells or mix culture of normal and RasV12-transformed cells. (C) Immunofluorescence images of AHNAK2. (D) Quantification of fluorescence intensity of AHNAK2. Values are expressed as a ratio relative to the average of MDCK alone. Cumulative data from 3 independent experiments are shown as means ± SDs. NS, not significant (unpaired 2-tailed Student's t test); n = 50 cells for each experiment.

(E–H) Effect of the pan-PKC inhibitor BIM-I or the Ca^{2+}-dependent conventional PKC inhibitor Go6976 on the phosphorylation of AHNAK2 (E and F) or the PKC substrate (G and H). (E and G) Immunofluorescence images of p-AHNAK2 (E) or p-PKC substrate (G) in the absence or presence of BIM-I or Go6976. (F and H)

(legend continued on next page)

antibody, AHNAK2 immunofluorescence was not altered in normal cells mix cultured with RasV12 cells (Figures 1C and 1D), suggesting that the level of AHNAK2 proteins in normal cells is not affected by mix culture with RasV12 cells. To validate these immunofluorescence analyses, we next established AHNAK2-knockout MDCK cells (Figure S2C). When AHNAK2-knockout cells were mix cultured with RasV12 cells, the increased immunofluorescence was not observed using anti-phospho-AHNAK2 antibody (Figure S2D). In addition, immunofluorescence with anti-AHNAK2 antibody was diminished in AHNAK2-knockout cells (Figure S2E), confirming the validity of both phospho-AHNAK2 and AHNAK2 immunofluorescence. Furthermore, we also found that the phosphorylation of AHNAK2 was enhanced in normal cells mix cultured with Src-transformed cells (Figures S2F and S2G). Collectively, these results indicate that phosphorylation of AHNAK2 is elevated in normal cells mix cultured with transformed cells at the early phase of cell competition.

Calcium-dependent conventional protein kinase C (PKC) acts upstream of AHNAK2 phosphorylation

To explore the upstream kinase for the AHNAK2 phosphorylation, we examined the effect of various kinase inhibitors. Addition of an inhibitor for Rho kinase (Y27632), phosphatidylinositol (PI)3 kinase (LY294002), c-Jun N-terminal kinase (JNK) (SP600125), or mitogen-activated protein kinase kinase (MEK) (U0216) did not affect the elevated AHNAK2 phosphorylation in normal cells mix cultured with RasV12-transformed cells (Figure S2H; data not shown). In contrast, the level of AHNAK2 phosphorylation was strongly suppressed by the pan-PKC inhibitor BIM-I or the Ca^{2+}-dependent conventional PKC inhibitor Go6976 (Figures 1E and 1F). Furthermore, to detect PKC activity, we used an antibody against a phosphorylated consensus sequence recognized by PKC (Sato et al., 2020). Immunofluorescence analysis showed that activity of PKC was elevated in normal cells mix cultured with RasV12 cells, which was diminished by BIM-I or Go6976 (Figures 1G and 1H). Moreover, the calcium ionophore ionomycin promoted the phosphorylation of AHNAK2, which was suppressed by Go6976 (Figure S2I). These results suggest that calcium-dependent conventional PKC acts upstream of the AHNAK2 phosphorylation.

Calcium sparks are induced in normal cells mix cultured with RasV12 cells via the mechanosensitive calcium channel TRPC1

To dynamically monitor the intracellular calcium level, we next used MDCK epithelial cells stably expressing GCaMP6s, a GFP-based intracellular calcium sensor (Chen et al., 2013; Nakai et al., 2001; Takeuchi et al., 2020). When GCaMP6s-expressing cells were mix cultured with normal cells, the GCaMP6s fluorescence intensity remained at a low level (Figures 2A and S3A; Video S1). In contrast, when GCaMP6s-expressing cells were mix cultured with RasV12 cells, transient upsurges in the GCaMP6s fluorescence were frequently observed within the epithelial layer (Figures 2B and S3B; Video S2), which we call "calcium sparks." For the quantification analysis, we defined the occurrence of calcium spark when the intensity of GCaMP surpassed the mean + 5 standard deviations (SDs) (Figures S3A and S3B: red line). The frequency of calcium sparks was significantly increased in GCaMP6s-expressing cells mix cultured with RasV12 cells (Figure 2C). Calcium sparks did not frequently occur in GCaMP6s-expressing RasV12 cells mix cultured with normal or RasV12 cells (Figure 2C). Calcium sparks were also observed in normal EpH4 murine mammary epithelial cells when they were mix cultured with RasV12-transformed EpH4 cells, but not with only GFP-expressing EpH4 cells (Figures S3C and S3D). To understand the molecular mechanism of calcium sparks, we next examined the effect of inhibitors for plasma membrane calcium channels. The addition of the mechanosensitive calcium channel inhibitor GsMTx profoundly suppressed the phosphorylation of AHNAK2 in normal cells mix cultured with RasV12 cells, whereas the L-type calcium channel inhibitor amlodipine had no effect (Figures 2D, 2E, S3E, and S3F). In addition, GsMTx also decreased the frequency of calcium sparks (Figure 2F; Video S3). GsMTx suppresses mechanosensitive calcium channels such as transient receptor potential (TRP) C1 and Piezo1. When TRPC1-knockdown cells were mix cultured with RasV12 cells, the increased phosphorylation of AHNAK2 or PKC substrate was not observed (Figures 2G, 2H, and S3G). Furthermore, TRPC1-knockdown significantly suppressed the frequency of calcium sparks (Figure 2I), whereas Piezo1-knockdown had no effect (data not shown). Collectively, these data indicate that when normal cells are mix cultured with RasV12 cells, calcium sparks are frequently induced via TRPC1. TRPC1 is a stretch-activated mechanosensitive calcium channel (Maroto et al., 2005). When stretching forces were applied to the monolayer of GCaMP-expressing MDCK cells cultured on the stretchable polydimethylsiloxane (PDMS) membrane, the GCaMP intensity was transiently elevated at 0.5 min upon stretching (Figure S3H). In addition, upon stretching, the phosphorylation of AHNAK2 was elevated at 10 min, and the phosphorylation level was kept at 30 or 60 min (Figures S3I and S3J; data not shown), suggesting that AHNAK2 phosphorylation can be maintained at a high level for a longer period. Furthermore, TRPC1-knockdown profoundly suppressed both the GCaMP intensity and AHNAK2 phosphorylation (Figures S3H–S3J). These results imply that membrane stretching induces TRPC1-mediated calcium influx, leading to AHNAK2 phosphorylation.

A recent study demonstrated that the activity of Cdc42 is enhanced across the wide areas of normal cells surrounding RasV12 cells (Kamasaki et al., 2021). Accordingly, we showed that the Cdc42 inhibitor ML141, but not the Rho inhibitor C3 transferase, significantly suppressed the phosphorylation of

Quantification of the fluorescence intensity of p-AHNAK2 (F) or p-PKC substrate (H). Values are expressed as a ratio relative to the average of MDCK alone (DMSO). (F) Data are means ± SDs from 3 independent experiments. (H) Cumulative data from 3 independent experiments are shown as means ± SDs. ****$p < 0.0001$ (1-way ANOVA with Dunnett's test); n = 50 cells for each experiment.
(A, C, E, and G) Scale bars, 20 μm.
See also Figures S1, S2, and Table S1.

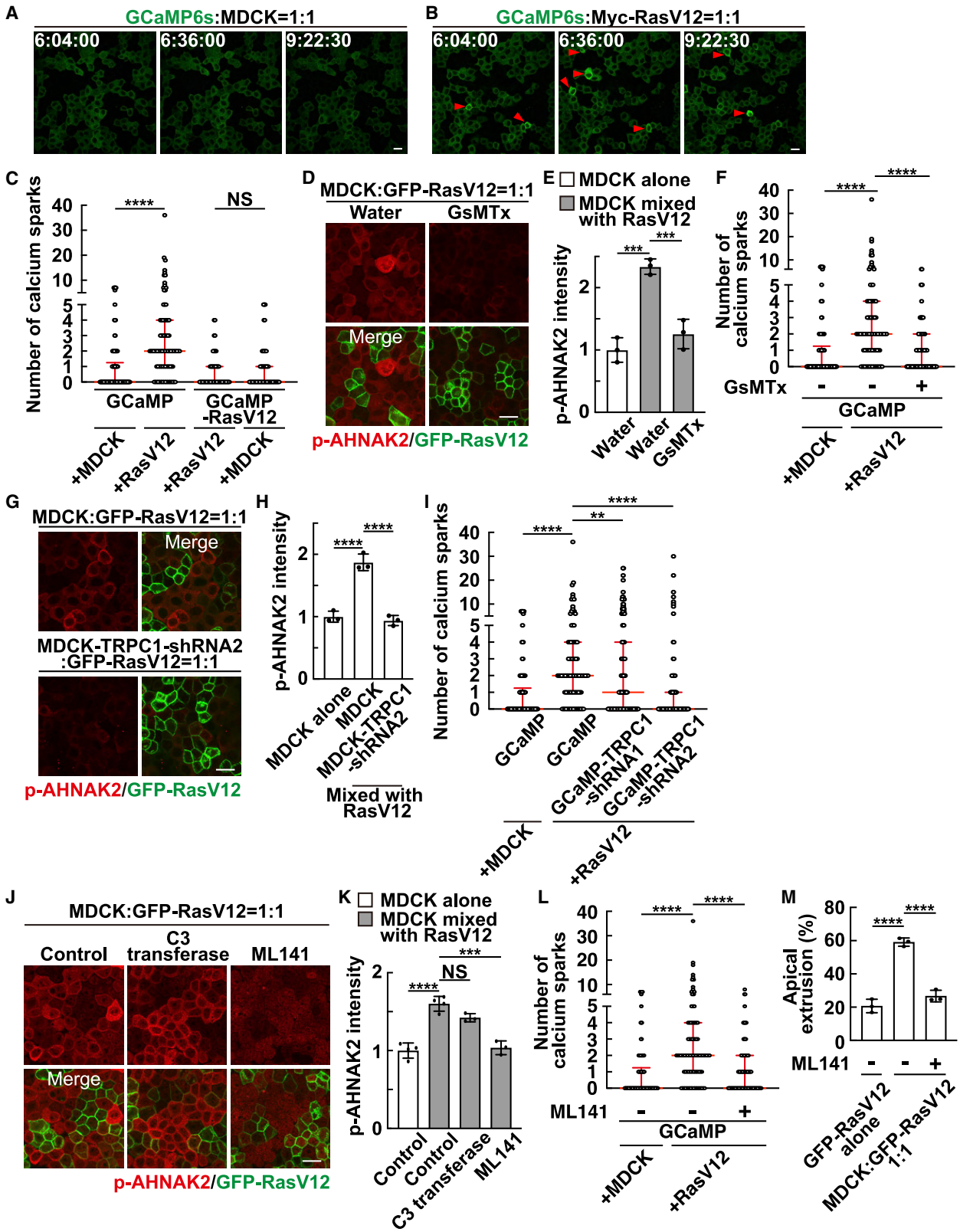

(legend on next page)

AHNAK2 in normal cells mix cultured with RasV12 cells (Figures 2J and 2K). N-WASP is one of the Cdc42 target proteins, and the N-WASP inhibitor Wiskostatin also diminished AHNAK2 phosphorylation (Figures S3K and S3L). In addition, the ML141 treatment or the expression of the dominant-negative mutant of Cdc42 (Cdc42T17N) in normal cells suppressed the frequency of calcium sparks (Figures 2L and S3M). Moreover, apical extrusion of RasV12 cells was profoundly suppressed by ML141 (Figure 2M). Collectively, these data indicate that Cdc42 is a crucial upstream regulator for calcium sparks, AHNAK2 phosphorylation, and apical extrusion.

Mix culture with RasV12-transformed cells induces the morphological and mechanical changes in normal cells

To further explore the underlying molecular mechanisms of calcium sparks under the mix culture condition, we analyzed the morphological properties of cells. We found that the nuclear aspect ratio was substantially altered in normal cells mix cultured with RasV12 cells, compared with that in normal cells cultured alone (Figures 3A and 3B). In addition, cell height was significantly increased in normal cells mix cultured with RasV12 cells (Figures 3A and 3C). The ML141 treatment suppressed the changes in the nuclear aspect ratio and cell height (Figures 3B and 3C), suggesting that Cdc42 is involved in those morphological changes. In contrast, the GsMTx treatment did not substantially influence the nuclear aspect ratio or cell height (Figures S4A and S4B). In the mix cultured condition, the cell area was similar between normal and RasV12 cells, which was lower than that in monocultured normal cells (Figure S4C). Under the 10:1 mix cultured condition, comparable changes were observed in the frequency of calcium sparks, nuclear aspect ratio, and cell height (Figures S4D–S4F). Furthermore, time-lapse analyses with 30-s intervals revealed that either the nuclear or cell aspect ratio frequently changed between 30-s time frames before and after calcium sparks in normal cells mix cultured with RasV12 cells (Figures 3D and 3E), indicating the dynamic morphological changes accompanied by calcium sparks. We next analyzed the cellular mechanical stress using traction force microscopy (TFM) and Bayesian inversion stress microscopy (BISM) (for details, see STAR Methods). We calculated the isotropic stress within the monolayers at 6–10 h after the induction of RasV12 expression. The isotropic stress gives us information about the constrained status of the tissue, in which a positive stress means that the tissue is under tension. Compared with the monoculture condition, normal cells were under smaller tension (lower isotropic stress values) when mix cultured with RasV12 cells (Figure 3F). The more compressed status of normal cells under the mix culture condition can lead to membrane stretching (Eisenhoffer et al., 2012; Valon and Levayer, 2019), which is consistent with their increased cell height (Figure 3C) (Rouven Bruckner et al., 2015). We then analyzed the mechanical state of plasma membranes using a membrane tension sensor Flipper-TR. Flipper-TR is a small molecule that intercalates into membranes, and the membrane tension can be monitored through changes in its fluorescence lifetime; the increased membrane tension leads to the elongated lifetime of Flipper-TR (Colom et al., 2018). Hyper- and hypo-osmotic treatments are supposed to decrease and increase plasma membrane tension, respectively. We showed that hyper- and hypo-osmotic treatments down- and upregulated, respectively, the Flipper-TR lifetime (Figures 3G and 3H), validating the usage of Flipper-TR as a membrane tension sensor for MDCK cells. We then measured the membrane

Figure 2. Calcium sparks are induced in normal cells mix cultured with RasV12 cells via the mechanosensitive calcium channel TRPC1

(A and B) Time-lapse analysis of calcium sparks in GCaMP-expressing normal cells mix cultured with normal cells (A) or RasV12-transformed cells (B). Representative images extracted from time-lapse imaging of MDCK-GCaMP6s cells mix cultured with normal MDCK cells (A) or MDCK-pTRE3G Myc-RasV12 cells (B) at a ratio of 1:1 during 6–10 h after the induction of RasV12 expression. The red arrowheads indicate calcium spark-positive cells.

(C) Quantification of the number of calcium sparks in MDCK-GCaMP6s cells or MDCK-pTRE3G Myc-RasV12-GCaMP6s cells mix cultured with normal MDCK or MDCK-pTRE3G Myc-RasV12 cells at a ratio of 1:1 during 6–10 h after the induction of RasV12 expression. Cumulative data from 3 (GCaMP) or 2 (GCaMP-RasV12) independent experiments are shown as medians ± IQRs (interquartile ranges). ****$p < 0.0001$ and NS, not significant (Kruskal-Wallis test with Dunn's test); n = 30 cells for each experiment.

(D and E) Effect of the mechanosensitive calcium channel inhibitor GsMTx on AHNAK2 phosphorylation. (D) Immunofluorescence images of p-AHNAK2 (red) in the absence or presence of GsMTx. (E) Quantification of the fluorescence intensity of p-AHNAK2. Values are expressed as a ratio relative to the average of MDCK alone (water). Data are means ± SDs from 3 independent experiments. ***$p < 0.001$ (1-way ANOVA with Dunnett's test); n = 50 cells for each experiment.

(F) Effect of GsMTx on the frequency of calcium sparks. Cumulative data from 3 independent experiments are shown as medians ± IQRs. ****$p < 0.0001$ (Kruskal-Wallis test with Dunn's test); n = 30 cells for each experiment.

(G and H) Effect of TRPC1-knockdown on AHNAK2 phosphorylation. (G) Immunofluorescence images of p-AHNAK2 (red). (H) Quantification of the fluorescence intensity of p-AHNAK2. Values are expressed as a ratio relative to the average of MDCK alone. Data are means ± SDs from 3 independent experiments. ****$p < 0.0001$ (1-way ANOVA with Dunnett's test); n = 50 cells for each experiment.

(I) Effect of TRPC1-knockdown on the frequency of calcium sparks. MDCK-GCaMP6s-TRPC1-shRNA1 or -shRNA2 cells were mix cultured with MDCK-pTRE3G Myc-RasV12 cells at a ratio of 1:1. Cumulative data from 4 (GCaMP-TRPC1-shRNA1) or 3 (the other conditions) independent experiments are shown as medians ± IQRs. **$p < 0.01$ and ****$p < 0.0001$ (Kruskal-Wallis test with Dunn's test); n = 30 cells for each experiment.

(J and K) Effect of the Rho inhibitor C3 transferase or the Cdc42 inhibitor ML141 on AHNAK2 phosphorylation. (J) Immunofluorescence images of p-AHNAK2 (red) in the absence or presence of C3 transferase or ML141. (K) Quantification of the fluorescence intensity of p-AHNAK2. Values are expressed as a ratio relative to the average of MDCK alone (control). Data are means ± SDs from 4 (control) or 3 (C3 transferase and ML141) independent experiments. ***$p < 0.001$, ****$p < 0.0001$, and NS, not significant (1-way ANOVA with Dunnett's test); n = 50 cells for each experiment.

(L) Effect of ML141 on the frequency of calcium sparks. Cumulative data from 3 independent experiments are shown as medians ± IQRs. ****$p < 0.0001$ (Kruskal-Wallis test with Dunn's test); n = 30 cells for each experimental condition.

(M) Effect of ML141 on apical extrusion of RasV12-transformed cells. At 24 h after RasV12 induction, the ratio of the apical extrusion was analyzed. Data are means ± SDs from 3 independent experiments. ****$p < 0.0001$ (1-way ANOVA with Dunnett's test); n > 250 cells for each experiment.

(A, B, D, G, and J) Scale bars, 20 μm.

See also Figure S3; Videos S1, S2, and S3.

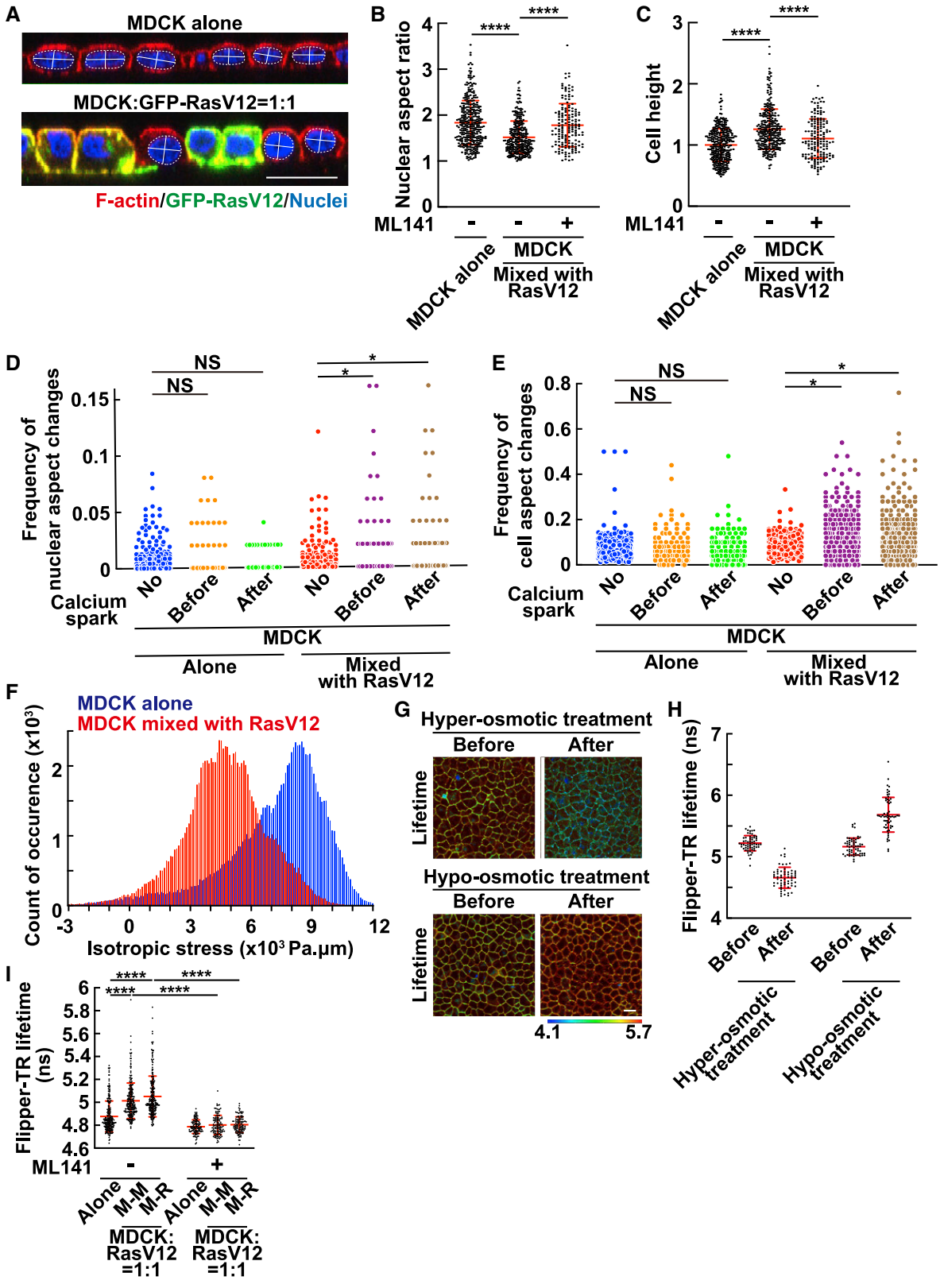

(legend on next page)

tension in the monoculture or mix culture. Compared with the monoculture condition of normal cells, the lifetime of Flipper-TR was increased at the boundaries between normal cells (M-M) or between normal and RasV12 cells (M-R) in the mix culture with RasV12 cells, which was suppressed by the ML141 treatment (Figure 3I), indicating that membrane tension is increased in normal cells mix cultured with RasV12-transformed cells, which is regulated by Cdc42.

INF2 induces perinuclear actin and AHNAK2 phosphorylation

We also realized that in normal MDCK cells mix cultured with RasV12-transformed MDCK cells, F-actin was often accumulated in the cytosol and perinuclear region (Figures 4A, 4B, and S4G). The comparable accumulation of perinuclear actin was also observed in normal EpH4 cells mix cultured with RasV12-transformed EpH4 cells (Figures 4C and 4D). Previous studies have demonstrated that transiently increased intracellular calcium can mediate perinuclear actin accumulation via inverted formin 2 (INF2) (Shao et al., 2015; Takeuchi et al., 2020; Wales et al., 2016). Indeed, knockdown of TRPC1 or knockout of INF2 strongly suppressed the ratio of perinuclear actin-positive cells, which was accompanied by the decreased cytosolic F-actin (Figures 4A, 4B, 4E, and 4F). INF2-knockout also diminished the phosphorylation of AHNAK2 or PKC substrate (Figures 4G–4J), but it did not decrease the frequency of calcium sparks (data not shown). These results suggest that TRPC1 and INF2 induce the accumulation of perinuclear actin, which somehow promotes AHNAK2 phosphorylation (Figure S6F).

Calcium sparks promote the tissue fluidity within the epithelial layer at the early phase of cell competition through INF2 and AHNAK2

We further investigated the functional significance of calcium sparks in cell competition. Previous studies have demonstrated that increased intracellular calcium via stretch-activated calcium channel can facilitate cell movement (Lee et al., 1999; Takeuchi et al., 2020; Wei et al., 2009). Thus, we examined the cell movement of normal and RasV12-transformed cells during the early phase of cell competition. Between 6 and 10 h of the induction of RasV12 expression, the displacement (L) of a centroid of normal or RasV12 cells was analyzed for each 1-h interval (Figure 5A), and the sum of the displacement distances for 4 h (4 intervals) was calculated. We then found that normal cells mix cultured with RasV12 cells moved further than normal cells cultured alone (Figure 5B). Furthermore, TRPC1-knockdown or INF2-knockout substantially diminished the movement of normal cells under the mix culture condition (Figure 5B). Intriguingly, RasV12 cells mix cultured with normal cells moved further than RasV12 cells cultured alone, and TRPC1-knockdown or INF2-knockout in normal cells suppressed the movement of RasV12 cells under the mix culture condition (Figure 5B). These results suggest that calcium sparks in normal cells promote the movement of normal cells as well as that of RasV12 cells. The frequency of cell division in normal cells was not affected by mix culture with RasV12 cells, indicating that cell division does not correlate with cell movement (Figure S5A). Moreover, AHNAK2-knockout or -knockdown in normal cells diminished the movement of both normal and RasV12 cells (Figures 5C, S5C, and S5D). To further examine the functional role of

Figure 3. Mix culture with RasV12-transformed cells induces morphological and mechanical changes in normal cells in a non-cell-autonomous manner

(A–C) The nuclear aspect ratio or cell height in normal cells mix cultured with RasV12-transformed cells. (A) The xz-immunofluorescence images of normal cells mix cultured with RasV12 cells. Normal MDCK cells were cultured alone or mix cultured with MDCK-pTR GFP-RasV12 cells at a ratio of 1:1, followed by staining with Alexa Fluor-568-phalloidin (red) and Hoechst (blue). The lines indicate the major and minor axes of the nucleus. (B and C) The nuclear aspect ratio (major axis/minor axis) (B) or cell height (C) in the absence or presence of ML141 was quantified from xz-confocal images. For cell height, values are expressed as a ratio relative to the average of MDCK alone. Cumulative data from 5 (absence of ML141) or 3 (presence of ML141) independent experiments are shown as means ± SDs. ****$p < 0.0001$ (1-way ANOVA with Dunnett's test); n = 355, 306, and 162 cells.

(D and E) Frequency of changes in the nuclear aspect ratio (D) or cell aspect ratio (E). MDCK-GCaMP6s cells were mix cultured with normal MDCK (MDCK alone) or MDCK-pTRE3G Myc-RasV12 cells (MDCK mixed with RasV12). Cells were stained with Hoechst and the far-red silicon rhodamine (SiR)-actin fluorescent probe, followed by time-lapse imaging with 30-s intervals during 6–10 h after the induction of RasV12 expression. The dynamic changes in the nuclear or cell aspect ratio before and after calcium sparks were analyzed. The triangle threshold algorithm was applied to obtain the threshold for morphological change points (for details, see STAR Methods). The values are expressed as a frequency of significant changes within each 30-s interval. Cumulative data from 2 independent experiments are shown. *$p < 0.05$ and NS, not significant (Wilcoxon signed sum test with Bonferroni correction). n = 414, 117, 117, 301, 283, and 283 cells.

(F) Isotropic stress in normal cells mix cultured with RasV12-transformed cells. MDCK-GCaMP6s cells were mix cultured with MDCK cells or MDCK-pTRE3G Myc-RasV12 at a ratio of 1:1 on a soft silicone elastomer substrate coated with fluorescent beads, which allowed us to measure the traction forces exerted by the cells on the underlying substrate using traction force microscopy (TFM). The traction forces were converted to intracellular stress inside the monolayer using Bayesian inversion stress microscopy (BISM). The isotropic stress in the monolayers at 6–10 h after the induction of RasV12 expression was calculated. The representative histograms are shown from 2 independent experiments. Binning of the histogram is presented every 100 Pa.μm, and the y axis indicates the count of occurrence in each bin.

(G and H) Effect of hyper- or hypo-osmotic treatment on the fluorescence lifetime of Flipper-TR. Normal MDCK cells were stained with the Flipper-TR membrane tension probe. The fluorescence lifetime of Flipper-TR was measured using fluorescence lifetime imaging microscopy (FLIM) before and after hyper-osmotic treatment for 20 min or hypo-osmotic treatment for 10 min. (G) Representative FLIM images of MDCK cells before and after hyper- or hypo-osmotic treatment. The color bar corresponds to lifetime (nanoseconds). (H) Quantification of Flipper-TR lifetime at cell-cell adhesions. Data are means ± SDs from 60 regions for each experiment.

(I) Effect of mix culture with RasV12-transformed cells on Flipper-TR lifetime. Flipper-TR lifetime at cell-cell adhesions between MDCK cells (M-M) or between MDCK and RasV12 cells (M-R) was analyzed. Cumulative data from 4 (absence of ML141) or 2 (presence of ML141) independent experiments are shown as means ± SDs. ****$p < 0.0001$ (1-way ANOVA with Tukey's test); n = 60 regions for each experiment.

(A and G) Scale bar, 20 μm.

See also Figure S4.

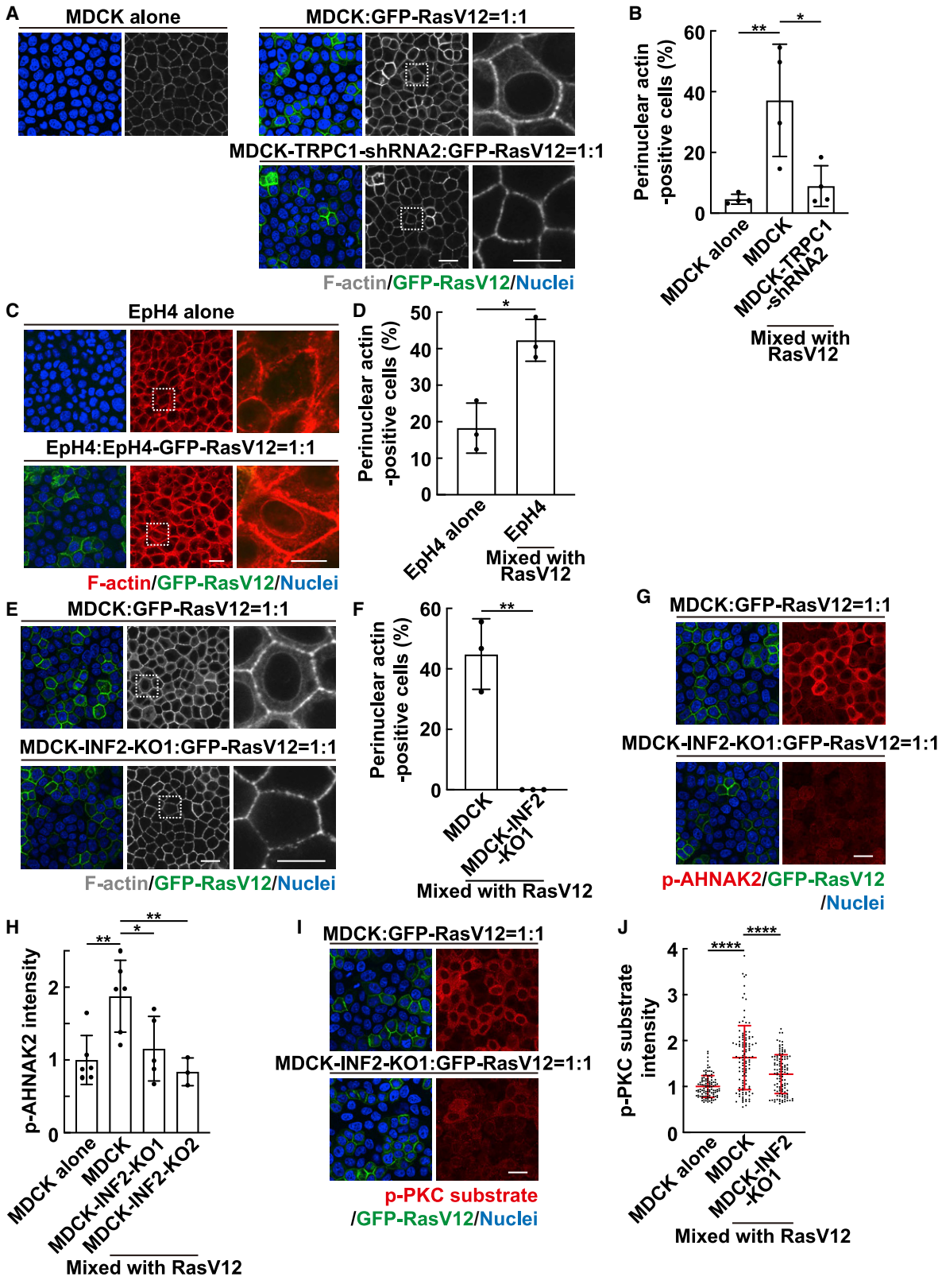

(legend on next page)

AHNAK2 phosphorylation, we established AHNAK2-knockout MDCK cells stably expressing WT AHNAK2 or non-phosphorylatable (SA) AHNAK2 (Figures S5E and S5F). We noticed that AHNAK2-knockout promoted the formation of actin stress fibers at the basal adhesion sites, and this AHNAK2-knockout phenotype was diminished by the expression of AHNAK2-WT, but not by that of AHNAK2-SA (Figure S5E). In addition, AHNAK2-WT, but not AHNAK2-SA, rescued the movement of both normal and RasV12 cells (Figures 5C and S5G). Apical extrusion of RasV12-transformed cells was enhanced by mix culture with normal cells (Figures 5D and S5H). Treatment with GsMTx at the early phase of cell competition suppressed the frequency of apical extrusion of RasV12 cells (Figure 5E). Moreover, AHNAK2-knockout in the surrounding cells suppressed apical extrusion of RasV12 cells, which was rescued by AHNAK2-WT, but not by AHNAK2-SA (Figure 5F). Collectively, these data indicate that calcium sparks enhance cell movements within the epithelial layer and facilitate apical extrusion of transformed cells through INF2 and AHNAK2.

Mechanosensitive calcium channel positively regulates calcium sparks, cell movement, and apical extrusion in zebrafish larvae as well

To investigate whether calcium sparks play a prevalent role in the early phase of cell competition between normal and RasV12-transformed cells, we examined zebrafish larvae (Figure 6A). When mKO2-RasV12 expression was induced within the outermost epithelial monolayer in a mosaic manner, apical extrusion of RasV12 cells was observed in the late somitogenesis stage (approximately 25 hpf) (Takeuchi et al., 2020). We then examined the GCaMP fluorescence in the epithelium at 18–20 hpf and found that calcium sparks indeed frequently occurred in the surrounding cells around RasV12-expressing cells, but not in RasV12 cells (Figures 6B–6D; Video S4). Calcium sparks were dominantly observed in the surrounding cells directly contacting RasV12 cells. When mKO2 alone was expressed, frequent calcium sparks were not observed (Figures 6B–6D; Video S4). In addition, GsMTx treatment profoundly suppressed the frequency of calcium sparks around RasV12 cells (Figures 6B–6D; Video S4). Furthermore, RasV12 expression induced the increased movement of the surrounding cells, which was suppressed by GsMTx (Figures 6E–6G). GsMTx also diminished the movement of RasV12 cells (Figures 6F and 6G). In contrast, cell movement was not increased in the distantly located cells from RasV12 cells (Figures 6E and 6H). The frequency of cell division was not affected by the presence of the neighboring RasV12 cells, indicating that cell division does not correlate with cell movement (Figure S5B). Moreover, GsMTx treatment at 14–20 hpf suppressed the frequency of apical extrusion of RasV12 cells (Figures 6I and 6J). These data suggest that calcium sparks enhance the cell movement at the early phase of cell competition and promote apical elimination of transformed cells in zebrafish larvae as well.

DISCUSSION

It has been reported that various cellular processes occur at the late stage of cell competition between normal and RasV12-transformed epithelial cells (Figure S6A). For example, cytoskeletal proteins filamin and vimentin accumulate in normal cells at the interface with RasV12 cells (Kajita et al., 2014). In addition, Warburg effect-like metabolic changes occur in RasV12 cells surrounded by normal cells (Kon et al., 2017). Knockdown of filamin in normal cells diminishes the Warburg effect-like metabolic changes in RasV12 cells (Kon et al., 2017), demonstrating the non-cell-autonomous influences between normal and transformed cells. In this study, we demonstrate that calcium sparks occur during the earlier phase of cell competition in normal cells neighboring RasV12-transformed cells. The blockage of calcium sparks by GsMTx treatment significantly suppresses filamin accumulation (Figures S6B and S6C), implying that calcium sparks influence some, if not all, of the processes at the late stage of cell competition. In contrast, treatment with the gap junction inhibitor αGA, which does not affect calcium sparks but suppresses calcium wave, does not influence the frequency of filamin accumulation (Figures S6D and S6E), suggesting that calcium wave does not act upstream of filamin accumulation.

Calcium sparks promote the cell movement within the epithelial layer. The depletion of INF2 or AHNAK2 cancels the calcium spark-mediated cell movement, and INF2 and AHNAK2 are

Figure 4. INF2 induces perinuclear actin and AHNAK2 phosphorylation

(A and B) TRPC1-mediated perinuclear actin in normal cells mix cultured with RasV12-transformed cells. (A) Fluorescence images of perinuclear actin. Magnified images of the white dashed regions are shown at right. (B) Quantification of perinuclear actin-positive cells. Data are means ± SDs from 4 independent experiments. *p < 0.05 and **p < 0.01 (1-way ANOVA with Dunnett's test); n = 1,009, 672, and 719 cells.

(C and D) Perinuclear actin in EpH4 cells. (C) Fluorescence images of perinuclear actin. Magnified images of the white dashed regions are shown at right. (D) Quantification of perinuclear actin-positive cells. Data are means ± SDs from 3 independent experiments. *p < 0.05 (unpaired 2-tailed Student's t test); n = 885 and 488 cells.

(E and F) Effect of INF2-knockout (KO) on perinuclear actin. (E) Fluorescence images of perinuclear actin. Magnified images of the white dashed regions are shown at right. (F) Quantification of perinuclear actin-positive cells. Data are means ± SDs from 3 independent experiments. **p < 0.01 (unpaired 2-tailed Student's t test); n = 383 and 348 cells.

(G and H) Effect of INF2-KO on AHNAK2 phosphorylation. (G) Immunofluorescence images of p-AHNAK2. (H) Quantification of the immunofluorescence intensity of p-AHNAK2. Values are expressed as a ratio relative to the average of MDCK alone. Data are means ± SDs from 6 (MDCK alone and MDCK mixed with RasV12), 5 (MDCK-INF2-KO1 mixed with RasV12), or 3 (MDCK-INF2-KO2 mixed with RasV12) independent experiments. *p < 0.05 and **p < 0.01 (1-way ANOVA with Dunnett's test); n = 215, 215, 185, and 85 cells.

(I and J) Effect of INF2-KO on p-PKC substrate. (I) Immunofluorescence images of p-PKC substrate. (J) Quantification of the immunofluorescence intensity of p-PKC substrate. Values are expressed as a ratio relative to the average of MDCK alone. Cumulative data from 3 independent experiments are shown as means ± SDs. ****p < 0.0001 (1-way ANOVA with Dunnett's test); n = 110 cells for each experimental condition.

(A, C, E, G, and I) Scale bars, 20 and 10 μm (magnified images).

See also Figure S4.

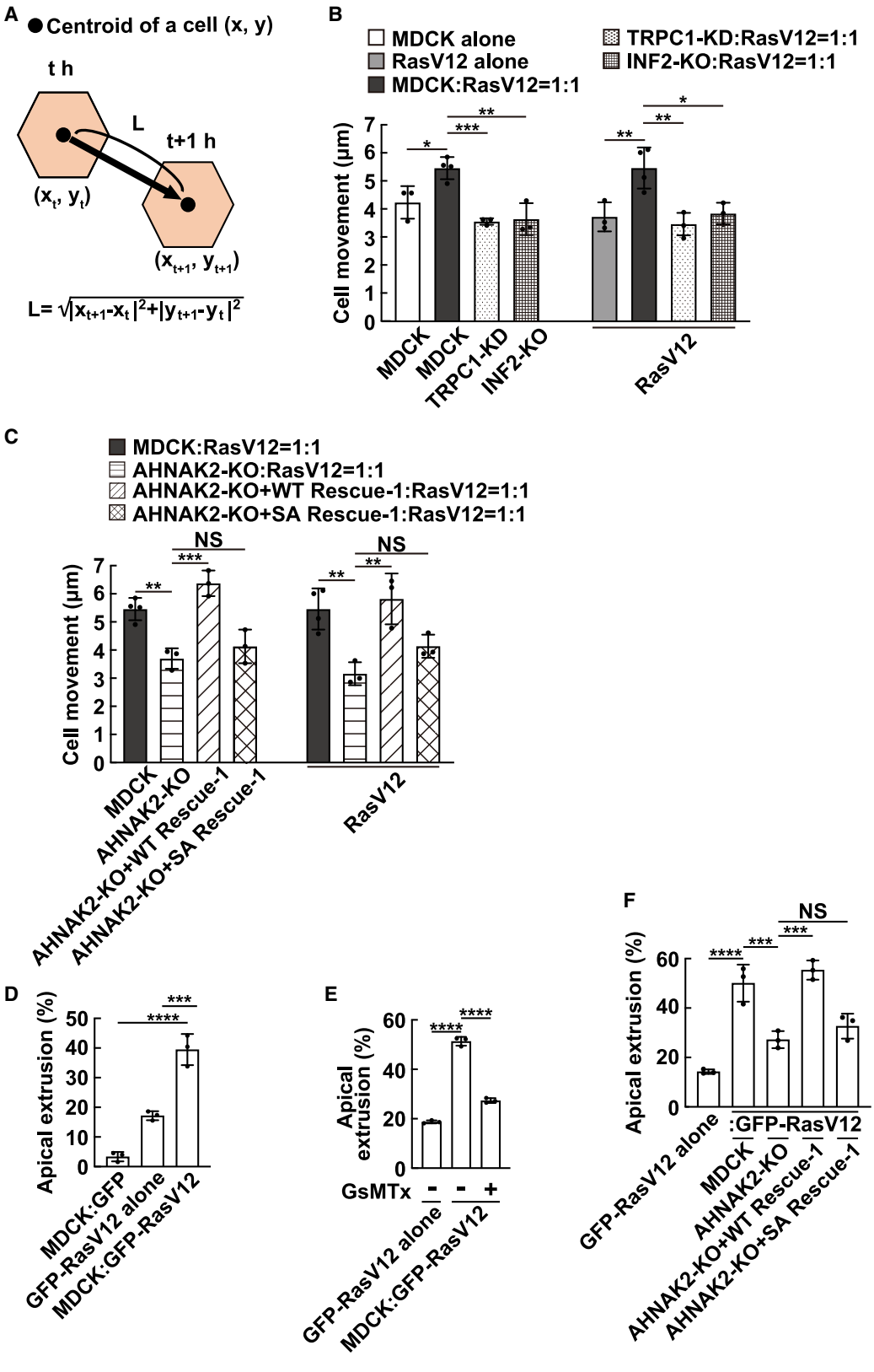

(legend on next page)

involved in the regulation of perinuclear actin and stress fibers respectively, suggesting that calcium sparks may affect the cell movement through the rearrangement of actin cytoskeletons by INF2 and AHNAK2. Then, how does the increased cell movement affect the cellular interactions? A previous study using atomic force microscopy (AFM) has demonstrated that RasV12-transformed cells have higher apparent cell viscosity and cortical elasticity than normal cells (Hogan et al., 2009). Mixing two cell groups with different physical properties can cause heterogeneous and imbalanced forces within the epithelial layer. The elevated cell movement may rectify and mitigate the distorted force balance. In addition, the increased tissue fluidity within the epithelial layer can also positively regulate cell competition between normal and RasV12 cells. In cell competition, the elimination of loser cells requires winner-loser cell mixing, and the increase in surface contacts between winners and losers promotes competition (Levayer et al., 2015). Cell sorting is another intercellular process by which cells with different physical properties (and/or cell adhesions) are segregated from each other, and each cell group forms aggregated cell clusters to decrease contacting areas between two different cell types (Krens and Heisenberg, 2011), which would suppress cell competition between them. Although different cortical elasticity between normal and RasV12 cells can cause cell sorting, we have found that the cell sorting process does not efficiently proceed and that the contacting areas are maintained between them over time (data not shown). Hence, it is plausible that the increased cell movement facilitates cell mixing and suppresses cell sorting between normal and transformed cells, thereby promoting cell competition. However, it is also possible that other (unidentified) downstream factors of calcium sparks and AHNAK2 may play additional roles in apical extrusion of RasV12 cells.

Previous studies have shown that during certain types of cell competition, loser cells receive compressive forces from the surrounding winner cells, which promote cell death and/or elimination of loser cells from the epithelial layer, a process called mechanical cell competition (Levayer et al., 2016; Wagstaff et al., 2016). In this study, the analyses of the cellular mechanical stress using TFM and BISM demonstrate that at the early phase of cell competition, compressive forces are imposed onto the surrounding normal (winner) cells, which may facilitate the process of apical extrusion of RasV12 cells. These results imply that mechanical forces can be regulated in both winner and loser cells in a non-cell-autonomous fashion during the course of cell competition.

AHNAK2 is an uncharacterized protein, and its function remains largely unknown. Canine AHNAK2 has six repeat domains in a central region, and a large portion of the respective repeat domains shares identical alignments of amino acid sequences (Figures S1F and S1G), implying that these highly resembling domains play a certain essential role for AHNAK2. The phosphorylation site identified in the phospho-SILAC screening lies within the repeat domains. The amino acid sequences near the phosphorylated serine residue are almost identical between the repeat domains, which are evolutionarily conserved in vertebrates. Therefore, it is technically infeasible to precisely identify by LC-MS/MS analysis which sites are phosphorylated, although most, if not all, serine residues could be phosphorylated simultaneously. Treatment with the pan-PKC inhibitor BIM-I or the Ca^{2+}-dependent conventional PKC inhibitor Go6976 suppresses the phosphorylation of AHNAK2, indicating that PKC is the upstream kinase for AHNAK2. Indeed, from the analysis with Netphos3.0 server networks to predict phosphorylation sites in eukaryotic proteins for 17 kinases (Blom et al., 2004), PKC is at the top among the predicted kinases for the phosphorylation sites of AHNAK2. However, it requires further investigation to tell whether AHNAK2 is a direct substrate of PKC. The results from the rescue experiments with AHNAK2-WT or AHNAK2-SA indicate that AHNAK2 phosphorylation regulates the cell movement. The underlying molecular mechanism is not understood yet, but according to the phenotype of AHNAK2-knockout and the rescue by exogenous AHNAK2 proteins, AHNAK2 may affect the cell movement through the regulation of F-actin stress fibers and cell adhesions. The functional role of AHNAK2 in cell competition needs to be investigated further in future studies.

Comparable calcium sparks, also called calcium spikes, have been observed in zebrafish, *Xenopus*, and *Drosophila*

Figure 5. Calcium sparks promote the epithelial tissue fluidity at the early phase of cell competition through the INF2-AHNAK2 pathway

(A) The schematic diagram for the displacement of the centroid of a cell. Black dots indicate the centroid of a cell (x, y). Using time-lapse imaging, cell movement was analyzed by calculating the displacement from the centroid of the cells at t h (x_t, y_t) to that at t + 1 h (x_{t+1}, y_{t+1}): the length of the black arrow ("L").

(B) Effect of TRPC1-knockdown or INF2-KO on cell movement. The total cell movement at 6–10 h after RasV12 induction was analyzed. Data are means ± SDs from 4 (MDCK:RasV12 = 1:1) or 3 (the other conditions) independent experiments. *p < 0.05, **p < 0.01, and ***p < 0.001 (1-way ANOVA with Dunnett's test); n = 30 cells for each experiment.

(C) Effect of the rescue of the expression of AHNAK2-WT (wild-type) or -SA (non-phosphorylatable form) into AHNAK2-KO cells on cell movement. Data are means ± SDs from 4 (MDCK:RasV12 = 1:1) or 3 (the other conditions) independent experiments. **p < 0.01, ***p < 0.001, and NS, not significant (1-way ANOVA with Dunnett's test); n = 30 cells for each experiment.

(D) Quantification of apical extrusion of RasV12-transformed cells mix cultured with normal cells. At 24 h after GFP or GFP-RasV12 induction, the ratio of apical extrusion was analyzed. Data are means ± SDs from 3 independent experiments. ***p < 0.001 and ****p < 0.0001 (1-way ANOVA with Dunnett's test); n > 250 cells for each experiment.

(E) Effect of the mechanosensitive calcium channel inhibitor GsMTx on apical extrusion of RasV12-transformed cells. Cells were cultured in the presence of GsMTx for 16 h after RasV12 induction, followed by the washout of GsMTx. At 24 h after RasV12 induction, the ratio of apical extrusion was analyzed. Data are means ± SDs from 3 independent experiments. ****p < 0.0001 (1-way ANOVA with Dunnett's test); n > 250 cells for each experiment.

(F) Effect of the rescue of AHNAK2-WT or -SA expression into AHNAK2-KO cells on apical extrusion. At 24 h after RasV12 induction, the ratio of apical extrusion was analyzed. Data are means ± SDs from 3 independent experiments. ***p < 0.001, ****p < 0.0001, and NS, not significant (1-way ANOVA with Tukey's test); n > 250 cells for each experiment.

See also Figure S5.

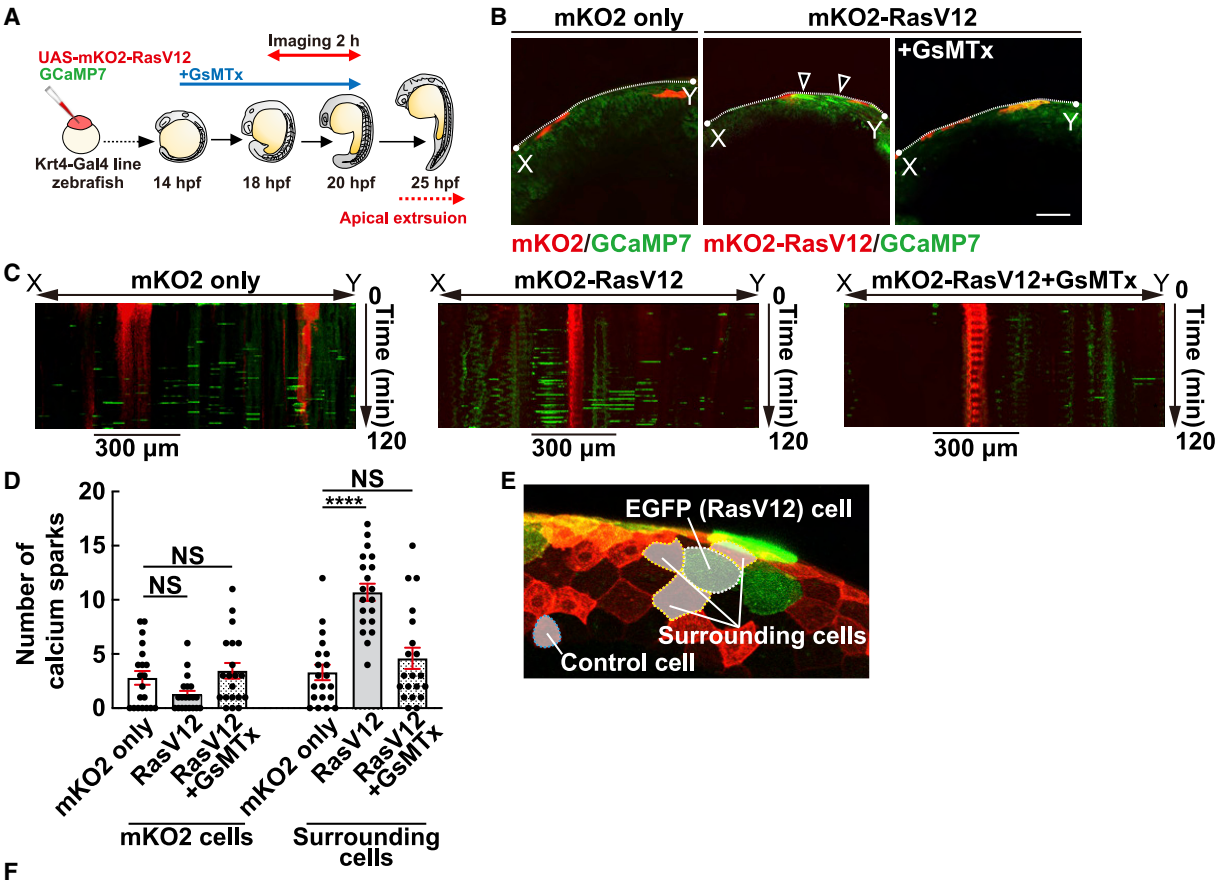

(legend on next page)

embryos (Ferrari and Spitzer, 1999; Leung et al., 2009; Markova et al., 2015; Reinhard et al., 1995; Shindo et al., 2010). The calcium spikes frequently occur during the tissue remodeling events in which cell forces and shape dynamically change. However, it remains obscure whether the calcium spikes are the cause or consequence of cell shape changes. Here, we show that during the early phase of the apical extrusion process, various morphological and physical changes are observed in normal cells mix cultured with RasV12-transformed cells; in particular, membrane tension is non-cell autonomously upregulated. In addition, the depletion of the stretch-activated calcium channel TRPC1 suppresses the frequency of calcium sparks, indicating that the increased membrane tension of normal cells causes calcium sparks. Then, how does the presence of neighboring RasV12 cells induce the increased membrane tension in normal cells? A recent study has shown that the Cdc42 activity is elevated in normal cells around RasV12 cells, leading to FBP17-mediated finger-like membrane protrusions (Kamasaki et al., 2021). Indeed, we have demonstrated that Cdc42 is a crucial upstream regulator for morphological changes, calcium sparks, AHNAK2 phosphorylation, and apical extrusion (Figure S6F). In future studies, the functional role of FBP17-mediated finger-like membrane protrusions should be explored further. Moreover, the further upstream mechanism of cell competition, especially the intercellular recognition machinery between normal and transformed cells, needs to be revealed.

Limitations of the study

In this study, we demonstrate that calcium sparks and AHNAK2 induce the increased cell movements of both normal and RasV12 cells under the mix culture condition and promote apical extrusion of RasV12 cells. However, some of the detailed, underlying molecular mechanisms still remain uncovered, which we would like to elucidate in future studies.

STAR★METHODS

Detailed methods are provided in the online version of this paper and include the following:

- KEY RESOURCES TABLE
- RESOURCE AVAILABILITY
  - Lead contact
  - Materials availability
  - Data and code availability
- EXPERIMENTAL MODEL AND SUBJECT DETAILS
  - Animals
  - Cell lines
- METHOD DETAILS
  - Antibodies, plasmids, and materials
  - Establishment of cell lines
  - Cell culture
  - Phospho-SILAC (stable isotope labeling with amino acids in cell culture) screening
  - LC-MS/MS analysis
  - Immunofluorescence and western blotting
  - Quantitative real-time PCR
  - Time-lapse observation of cultured cells
  - Stretching assay
  - Traction force microscopy and intracellular stress measurement
  - Membrane tension measurements by Flipper-TR
  - Zebrafish
- QUANTIFICATION AND STATISTICAL ANALYSIS
  - Statistical analysis

Figure 6. Mechanosensitive calcium channel positively regulates calcium sparks, cell movement, and apical extrusion in zebrafish larvae

(A) Schematic illustration of the experimental time course to observe calcium sparks before apical extrusion in zebrafish.

(B–D) Mechanosensitive calcium channel-mediated calcium sparks around RasV12-expressing cells in zebrafish larvae. (B) Fluorescence images of zebrafish 18-somite larvae expressing mKO2-RasV12 and GCaMP7 in the absence or presence of GsMTx. The result shown is the representative from 10 independent experiments. The arrowheads indicate calcium spark-positive cells. (C) Kymographs showing the calcium sparks (green) around RasV12-expressing cells (red). The area used for analysis (X-Y in B) is shown on the horizontal axis, and the time is shown on the vertical axis. (D) Quantification of the frequency of calcium sparks within 300 μm around RasV12-expressing cells or mKO2 only-expressing cells for 2 h in the absence or presence of GsMTx. Individual data points are plotted with the means ± SEMs. ****$p < 0.0001$ and NS, not significant (1-way ANOVA with Tukey's post-hoc multiple comparison test); n = 20 cells for each experimental condition.

(E–H) Effect of GsMTx on the cell movement in zebrafish larvae. (E) The cells used for the analysis of cell movement. A fluorescence image of zebrafish 18-somite larvae expressing EGFP-RasV12 and GAP43-mKO2. The white dotted line indicates an EGFP-RasV12 cell, while the yellow dotted line indicates surrounding normal cells expressing GAP43-mKO2. The blue dotted line indicates a cell distant from RasV12-expressing cells, which was used as control. (F) Fluorescence images of zebrafish 18-somite larvae expressing EGFP or EGFP-RasV12 and GAP43-mKO2 in the absence or presence of GsMTx. The trajectory of a cellular centroid shows the sum of the frame-to-frame distances for 2 h (12 frames at 10-min interval). The result shown is the representative from 10 independent experiments. (G) Quantification of the total distance of cell movement for 2 h. The RasV12-expressing cells and surrounding cells (as shown in E and F) were analyzed. Individual data points are plotted with the means ± SDs. ****$p < 0.0001$ and NS, not significant (2-way ANOVA with Tukey's post-hoc multiple comparison test); n = 18 cells for each experimental condition.

(H) Quantification of the total distance of cell movement of the control cells for 2 h. The control cells distant from RasV12-expressing cells (as shown in E) were analyzed. Individual data points are plotted with the means ± SDs. NS, not significant (2-way ANOVA with Tukey's post-hoc multiple comparison test); n = 18 cells for each experimental condition.

(I and J) Effect of the mechanosensitive calcium channel inhibitor GsMTx on apical extrusion of RasV12-transformed cells. (I) Fluorescence images of zebrafish larvae (24 hpf) expressing mKO2-RasV12 treated with or without GsMTx for 4 h. Black and white arrowheads indicate apically extruded and not-extruded mKO2-RasV12 cells, respectively. (J) Quantification of apical extrusion of RasV12-expressing cells at 24 hpf. Data are means ± SDs from 5 independent experiments. **$p < 0.01$ (2-tailed Student's t tests).

(B, F, and I) Scale bars, 100 μm.

See also Video S4.

SUPPLEMENTAL INFORMATION

Supplemental information can be found online at https://doi.org/10.1016/j.celrep.2022.111078.

ACKNOWLEDGMENTS

We acknowledge support from Japan Society for the Promotion of Science (JSPS) Grant-in-Aid for Scientific Research on Transformative Research Areas (A) 21H05285A01, Grant-in-Aid for Scientific Research (S) 21H05039, JSPS Bilateral Joint Research Projects (The Royal Society) JPJSBP1 20215703, JSPS Grant-in-Aid for Challenging Research (Pioneering) 20K21411, Japan Science and Technology Agency (JST) (Moonshot R&D: grant no. JPMJPS2022), the Takeda Science Foundation, and SAN-ESU GIKEN (to Y.F.), Grant-in-Aid for JSPS Research Fellow JP20J20930 (to K.K.) and JP21J01076 (to K.A.), the AMED PRIME program (20gm5810025h9904) (to K.S.), JSPS Grant-in-Aid for Scientific Research (B) 19H03412, AMED (JP20gm5010001), and JSPS Grant-in-Aid for Transformative Research Areas (A) 21H05287 (to T.I.), and JSPS Grant-in-Aid for Transformative Research Areas (A) 21H05291 (to S.T.). This work was also supported by the Kyoto University Live Imaging Center.

AUTHOR CONTRIBUTIONS

K.K., K.A., and K.I. designed the experiments and generated most of the data. M.Y., M.S., N.T., S. Iijima, S. Ishikawa, T.K., and S.T. assisted in the experiments using mammalian cell cultures. Y.A. and T.I. assisted in the experiments using zebrafish. T.H. performed the phospho-SILAC screening. K.Y., C.G.L., I.U., and H.I. analyzed the dynamic changes in the nuclear and cell aspect ratios. I.T. assisted in the statistical analyses. E.G. and K.S. performed the TFM experiments and analyzed the data. N.H. assisted in the Flipper-TR experiment. Y.F. conceived and designed the study. The manuscript was written by K.K., K.A., and Y.F., with assistance from the other authors.

DECLARATION OF INTERESTS

The authors declare no competing interests.

Received: January 21, 2022
Revised: May 13, 2022
Accepted: June 20, 2022
Published: July 12, 2022

REFERENCES

Amoyel, M., and Bach, E.A. (2014). Cell competition: how to eliminate your neighbours. Development *141*, 988–1000. https://doi.org/10.1242/dev.079129.

Baker, N.E. (2020). Emerging mechanisms of cell competition. Nat. Rev. Genet. *21*, 683–697. https://doi.org/10.1038/s41576-020-0262-8.

Blom, N., Sicheritz-Pontén, T., Gupta, R., Gammeltoft, S., and Brunak, S. (2004). Prediction of post-translational glycosylation and phosphorylation of proteins from the amino acid sequence. Proteomics *4*, 1633–1649. https://doi.org/10.1002/pmic.200300771.

Bowling, S., Lawlor, K., and Rodriguez, T.A. (2019). Cell competition: the winners and losers of fitness selection. Development *146*, dev167486.

Chen, T.W., Wardill, T.J., Sun, Y., Pulver, S.R., Renninger, S.L., Baohan, A., Schreiter, E.R., Kerr, R.A., Orger, M.B., Jayaraman, V., et al. (2013). Ultrasensitive fluorescent proteins for imaging neuronal activity. Nature *499*, 295–300. https://doi.org/10.1038/nature12354.

Colom, A., Derivery, E., Soleimanpour, S., Tomba, C., Molin, M.D., Sakai, N., González-Gaitán, M., Matile, S., and Roux, A. (2018). A fluorescent membrane tension probe. Nat. Chem. *10*, 1118–1125. https://doi.org/10.1038/s41557-018-0127-3.

Díaz-Díaz, C., and Torres, M. (2019). Insights into the quantitative and dynamic aspects of Cell Competition. Curr. Opin. Cell. Biol. *60*, 68–74. https://doi.org/10.1016/j.ceb.2019.04.003.

Eisenhoffer, G.T., Loftus, P.D., Yoshigi, M., Otsuna, H., Chien, C.B., Morcos, P.A., and Rosenblatt, J. (2012). Crowding induces live cell extrusion to maintain homeostatic cell numbers in epithelia. Nature *484*, 546–549. https://doi.org/10.1038/nature10999.

Ferrari, M.B., and Spitzer, N.C. (1999). Calcium signaling in the developing Xenopus myotome. Dev. Biol. *213*, 269–282. https://doi.org/10.1006/dbio.1999.9387.

Haraoka, Y., Akieda, Y., Nagai, Y., Mogi, C., and Ishitani, T. (2022). Zebrafish imaging reveals TP53 mutation switching oncogene-induced senescence from suppressor to driver in primary tumorigenesis. Nat. Commun. *13*, 1417. https://doi.org/10.1038/s41467-022-29061-6.

Hogan, C., Dupré-Crochet, S., Norman, M., Kajita, M., Zimmermann, C., Pelling, A.E., Piddini, E., Baena-López, L.A., Vincent, J.P., Itoh, Y., et al. (2009). Characterization of the interface between normal and transformed epithelial cells. Nat. Cell. Biol. *11*, 460–467. https://doi.org/10.1038/ncb1853.

Hogan, C., Serpente, N., Cogram, P., Hosking, C.R., Bialucha, C.U., Feller, S.M., Braga, V.M.M., Birchmeier, W., and Fujita, Y. (2004). Rap1 regulates the formation of E-cadherin-based cell-cell contacts. Mol. Cell. Biol. *24*, 6690–6700. https://doi.org/10.1128/mcb.24.15.6690-6700.2004.

Hsu, P.D., Scott, D.A., Weinstein, J.A., Ran, F.A., Konermann, S., Agarwala, V., Li, Y., Fine, E.J., Wu, X., Shalem, O., et al. (2013). DNA targeting specificity of RNA-guided Cas9 nucleases. Nat. Biotechnol. *31*, 827–832. https://doi.org/10.1038/nbt.2647.

Johnston, L.A. (2009). Competitive interactions between cells: death, growth, and geography. Science *324*, 1679–1682. https://doi.org/10.1126/science.1163862.

Kajita, M., Hogan, C., Harris, A.R., Dupre-Crochet, S., Itasaki, N., Kawakami, K., Charras, G., Tada, M., and Fujita, Y. (2010). Interaction with surrounding normal epithelial cells influences signalling pathways and behaviour of Src-transformed cells. J. Cell. Sci. *123*, 171–180. https://doi.org/10.1242/jcs.057976.

Kajita, M., Sugimura, K., Ohoka, A., Burden, J., Suganuma, H., Ikegawa, M., Shimada, T., Kitamura, T., Shindoh, M., Ishikawa, S., et al. (2014). Filamin acts as a key regulator in epithelial defence against transformed cells. Nat. Commun. *5*, 4428. https://doi.org/10.1038/ncomms5428.

Kamasaki, T., Miyazaki, Y., Ishikawa, S., Hoshiba, K., Kuromiya, K., Tanimura, N., Mori, Y., Tsutsumi, M., Nemoto, T., Uehara, R., et al. (2021). FBP17-mediated finger-like membrane protrusions in cell competition between normal and RasV12-transformed cells. iScience *24*, 102994. https://doi.org/10.1016/j.isci.2021.102994.

Kenry, Leong, M.C., Nai, M.H., Cheong, F.C., and Lim, C.T. (2015). Viscoelastic effects of silicone gels at the micro- and nanoscale. Procedia IUTAM *12*, 20–30. https://doi.org/10.1016/j.piutam.2014.12.004.

Kim, S.J., Koh, K., Boyd, S., and Gorinevsky, D. (2009). ℓ_1 trend filtering. SIAM Rev. *51*, 339–360. https://doi.org/10.1137/070690274.

Kon, S., Ishibashi, K., Katoh, H., Kitamoto, S., Shirai, T., Tanaka, S., Kajita, M., Ishikawa, S., Yamauchi, H., Yako, Y., et al. (2017). Cell competition with normal epithelial cells promotes apical extrusion of transformed cells through metabolic changes. Nat. Cell. Biol. *19*, 530–541. https://doi.org/10.1038/ncb3509.

Krens, S.F.G., and Heisenberg, C.P. (2011). Cell sorting in development. Curr. Top. Dev. Biol. *95*, 189–213. https://doi.org/10.1016/B978-0-12-385065-2.00006-2.

Lee, J., Ishihara, A., Oxford, G., Johnson, B., and Jacobson, K. (1999). Regulation of cell movement is mediated by stretch-activated calcium channels. Nature *400*, 382–386. https://doi.org/10.1038/22578.

Leung, C.F., Miller, A.L., Korzh, V., Chong, S.W., Sleptsova-Freidrich, I., and Webb, S.E. (2009). Visualization of stochastic Ca2+ signals in the formed somites during the early segmentation period in intact, normally developing zebrafish embryos. Dev. Growth. Differ. *51*, 617–637. https://doi.org/10.1111/j.1440-169x.2009.01123.x.

Leung, C.T., and Brugge, J.S. (2012). Outgrowth of single oncogene-expressing cells from suppressive epithelial environments. Nature *482*, 410–413. https://doi.org/10.1038/nature10826.

Levayer, R. (2020). Solid stress, competition for space and cancer: the opposing roles of mechanical cell competition in tumour initiation and growth. Semin. Cancer Biol. *63*, 69–80. https://doi.org/10.1016/j.semcancer.2019.05.004.

Levayer, R., Dupont, C., and Moreno, E. (2016). Tissue crowding induces caspase-dependent competition for space. Curr. Biol. *26*, 670–677. https://doi.org/10.1016/j.cub.2015.12.072.

Levayer, R., Hauert, B., and Moreno, E. (2015). Cell mixing induced by myc is required for competitive tissue invasion and destruction. Nature *524*, 476–480. https://doi.org/10.1038/nature14684.

Madan, E., Gogna, R., and Moreno, E. (2018). Cell competition in development: information from flies and vertebrates. Curr. Opin. Cell. Biol. *55*, 150–157. https://doi.org/10.1016/j.ceb.2018.08.002.

Markova, O., and Lenne, P.F. (2012). Calcium signaling in developing embryos: focus on the regulation of cell shape changes and collective movements. Semin. Cell. Dev. Biol. *23*, 298–307. https://doi.org/10.1016/j.semcdb.2012.03.006.

Markova, O., Sénatore, S., Chardès, C., and Lenne, P.F. (2015). Calcium Spikes in Epithelium: study on Drosophila early embryos. Sci. Rep. *5*, 11379. https://doi.org/10.1038/srep11379.

Maroto, R., Raso, A., Wood, T.G., Kurosky, A., Martinac, B., and Hamill, O.P. (2005). TRPC1 forms the stretch-activated cation channel in vertebrate cells. Nat. Cell. Biol. *7*, 179–185. https://doi.org/10.1038/ncb1218.

Martiel, J.L., Leal, A., Kurzawa, L., Balland, M., Wang, I., Vignaud, T., Tseng, Q., and Thery, M. (2015). Measurement of cell traction forces with ImageJ. Methods Cell. Biol. *125*, 269–287. https://doi.org/10.1016/bs.mcb.2014.10.008.

Maruyama, T., and Fujita, Y. (2017). Cell competition in mammals - novel homeostatic machinery for embryonic development and cancer prevention. Curr. Opin. Cell. Biol. *48*, 106–112. https://doi.org/10.1016/j.ceb.2017.06.007.

Masuda, T., Tomita, M., and Ishihama, Y. (2008). Phase transfer surfactant-aided trypsin digestion for membrane proteome analysis. J. Proteome Res. *7*, 731–740. https://doi.org/10.1021/pr700658q.

Morata, G., and Calleja, M. (2020). Cell competition and tumorigenesis in the imaginal discs of Drosophila. Semin. Cancer Biol. *63*, 19–26. https://doi.org/10.1016/j.semcancer.2019.06.010.

Morata, G., and Ripoll, P. (1975). Minutes: mutants of drosophila autonomously affecting cell division rate. Dev. Biol. *42*, 211–221. https://doi.org/10.1016/0012-1606(75)90330-9.

Nakai, J., Ohkura, M., and Imoto, K. (2001). A high signal-to-noise Ca(2+) probe composed of a single green fluorescent protein. Nat. Biotechnol. *19*, 137–141. https://doi.org/10.1038/84397.

Naruse, K., Yamada, T., Sai, X.R., Hamaguchi, M., and Sokabe, M. (1998). Pp125FAK is required for stretch dependent morphological response of endothelial cells. Oncogene *17*, 455–463. https://doi.org/10.1038/sj.onc.1201950.

Nier, V., Jain, S., Lim, C.T., Ishihara, S., Ladoux, B., and Marcq, P. (2016). Inference of internal stress in a cell monolayer. Biophys. J. *110*, 1625–1635. https://doi.org/10.1016/j.bpj.2016.03.002.

Ohoka, A., Kajita, M., Ikenouchi, J., Yako, Y., Kitamoto, S., Kon, S., Ikegawa, M., Shimada, T., Ishikawa, S., and Fujita, Y. (2015). EPLIN is a crucial regulator for extrusion of RasV12-transformed cells. J. Cell. Sci. *128*, 781–789. https://doi.org/10.1242/jcs.163113.

Olsen, J.V., Blagoev, B., Gnad, F., Macek, B., Kumar, C., Mortensen, P., and Mann, M. (2006). Global, in vivo, and site-specific phosphorylation dynamics in signaling networks. Cell *127*, 635–648. https://doi.org/10.1016/j.cell.2006.09.026.

Reinhard, E., Yokoe, H., Niebling, K.R., Allbritton, N.L., Kuhn, M.A., and Meyer, T. (1995). Localized calcium signals in early zebrafish development. Dev. Biol. *170*, 50–61. https://doi.org/10.1006/dbio.1995.1194.

Rouven Brückner, B., Pietuch, A., Nehls, S., Rother, J., and Janshoff, A. (2015). Ezrin is a major regulator of membrane tension in epithelial cells. Sci. Rep. *5*, 14700. https://doi.org/10.1038/srep14700.

Sasaki, A., Nagatake, T., Egami, R., Gu, G., Takigawa, I., Ikeda, W., Nakatani, T., Kunisawa, J., and Fujita, Y. (2018). Obesity suppresses cell-competition-mediated apical elimination of RasV12-transformed cells from epithelial tissues. Cell Rep. *23*, 974–982. https://doi.org/10.1016/j.celrep.2018.03.104.

Sato, N., Yako, Y., Maruyama, T., Ishikawa, S., Kuromiya, K., Tokuoka, S.M., Kita, Y., and Fujita, Y. (2020). The COX-2/PGE2 pathway suppresses apical elimination of RasV12-transformed cells from epithelia. Commun. Biol. *3*, 132. https://doi.org/10.1038/s42003-020-0847-y.

Shao, X., Li, Q., Mogilner, A., Bershadsky, A.D., and Shivashankar, G.V. (2015). Mechanical stimulation induces formin-dependent assembly of a perinuclear actin rim. Proc. Natl. Acad. Sci. USA *112*, E2595–E2601. https://doi.org/10.1073/pnas.1504837112.

Shindo, A., Hara, Y., Yamamoto, T.S., Ohkura, M., Nakai, J., and Ueno, N. (2010). Tissue-tissue interaction-triggered calcium elevation is required for cell polarization during Xenopus gastrulation. PLoS One *5*, e8897. https://doi.org/10.1371/journal.pone.0008897.

Swinburne, I.A., Mosaliganti, K.R., Green, A.A., and Megason, S.G. (2015). Improved long-term imaging of embryos with genetically encoded alpha-bungarotoxin. PLoS One *10*, e0134005. https://doi.org/10.1371/journal.pone.0134005.

Takeuchi, Y., Narumi, R., Akiyama, R., Vitiello, E., Shirai, T., Tanimura, N., Kuromiya, K., Ishikawa, S., Kajita, M., Tada, M., et al. (2020). Calcium wave promotes cell extrusion. Curr. Biol. *30*, 670–681.e6. https://doi.org/10.1016/j.cub.2019.11.089.

Tseng, Q., Duchemin-Pelletier, E., Deshiere, A., Balland, M., Guillou, H., Filhol, O., and Théry, M. (2012). Spatial organization of the extracellular matrix regulates cell-cell junction positioning. Proc. Natl. Acad. Sci. USA *109*, 1506–1511. https://doi.org/10.1073/pnas.1106377109.

Valon, L., and Levayer, R. (2019). Dying under pressure: cellular characterisation and in vivo functions of cell death induced by compaction. Biol. Cell *111*, 51–66. https://doi.org/10.1111/boc.201800075.

van der Walt, S., Schönberger, J.L., Nunez-Iglesias, J., Boulogne, F., Warner, J.D., Yager, N., Gouillart, E., Yu, T., and scikit-image, c. (2014). scikit-image: image processing in Python. PeerJ *2*, e453. https://doi.org/10.7717/peerj.453.

Vishwakarma, M., and Piddini, E. (2020). Outcompeting cancer. Nat. Rev. Cancer. *20*, 187–198. https://doi.org/10.1038/s41568-019-0231-8.

Wagstaff, L., Goschorska, M., Kozyrska, K., Duclos, G., Kucinski, I., Chessel, A., Hampton-O'Neil, L., Bradshaw, C.R., Allen, G.E., Rawlins, E.L., et al. (2016). Mechanical cell competition kills cells via induction of lethal p53 levels. Nat. Commun. *7*, 11373. https://doi.org/10.1038/ncomms11373.

Wales, P., Schuberth, C.E., Aufschnaiter, R., Fels, J., García-Aguilar, I., Janning, A., Dlugos, C.P., Schäfer-Herte, M., Klingner, C., Wälte, M., et al. (2016). Calcium-mediated actin reset (CaAR) mediates acute cell adaptations. Elife *5*, e19850. https://doi.org/10.7554/elife.19850.

Wang, Y., Yang, F., Gritsenko, M.A., Wang, Y., Clauss, T., Liu, T., Shen, Y., Monroe, M.E., Lopez-Ferrer, D., Reno, T., et al. (2011). Reversed-phase chromatography with multiple fraction concatenation strategy for proteome profiling of human MCF10A cells. Proteomics *11*, 2019–2026. https://doi.org/10.1002/pmic.201000722.

Wei, C., Wang, X., Chen, M., Ouyang, K., Song, L.S., and Cheng, H. (2009). Calcium flickers steer cell migration. Nature *457*, 901–905. https://doi.org/10.1038/nature07577.

Wu, S.K., Gomez, G.A., Michael, M., Verma, S., Cox, H.L., Lefevre, J.G., Parton, R.G., Hamilton, N.A., Neufeld, Z., and Yap, A.S. (2014). Cortical F-actin stabilization generates apical-lateral patterns of junctional contractility that integrate cells into epithelia. Nat. Cell. Biol. *16*, 167–178. https://doi.org/10.1038/ncb2900.

Zack, G.W., Rogers, W.E., and Latt, S.A. (1997). Automatic mesurement of sister chromatid exchange frequency. J. Histochem. Cytochem. *25*, 741–753.

STAR★METHODS

KEY RESOURCES TABLE

REAGENT or RESOURCE	SOURCE	IDENTIFIER
Antibodies		
Rabbit anti-phospho-AHNAK2 antibody	This paper	N/A
Rabbit anti-AHNAK2 antibody	This paper	N/A
Mouse anti-FLAG (M2) antibody	Sigma-Aldrich	Cat# F3165; RRID:AB_259529
Mouse anti-Actin antibody, clone C4	Millipore	Cat# MAB1501R clone C4; RRID:AB_2223041
Mouse anti-GFP antibody	Roche	Cat# 11814460001; RRID:AB_390913
Rabbit anti-phospho-(Ser) PKC Substrate antibody	Cell Signaling Technology	Cat# 2261; RRID:AB_330310
Mouse Anti-Pan-Ras (Ab-3)	Millipore	Cat# OP40; RRID:AB_213400
Horseradish peroxidase-conjugated AffiniPure anti-mouse IgG	Jackson ImmunoResearch	Cat# 715-035-151
Alexa Fluor 568 Anti-rabbit	Thermo Fisher	Cat# A21069; RRID: AB_10563601
Alexa Fluor 568 Anti-mouse	Thermo Fisher	Cat# A10037; RRID:AB_2534013
Alexa Fluor 488 Anti-mouse	Thermo Fisher	Cat# A21202; RRID:AB_141607
Alexa Fluor-488-conjugated phalloidin	Life technologies	Cat# A12379
Alexa Fluor-568-conjugated phalloidin	Life technologies	Cat# A12380
Alexa Fluor-647-conjugated phalloidin	Life technologies	Cat# 22,287
Chemicals, peptides, and recombinant proteins		
Amlodipine besylate	Sigma-Aldrich	Cat# A5605
Wiskostatin	Sigma-Aldrich	Cat#W2270
18α-Glycyrrhetinic acid	Sigma-Aldrich	Cat# G8503
Go6976	Sigma-Aldrich	Cat# G1171
SP600125	Sigma-Aldrich	Cat# S5567
GsMTx (MDCK)	PEPTIDE INSTITUTE	Cat# 4393s
Ionomycin	FUJIFILM WAKO Pure Chemical Corporation	Cat# 095-05831
Bisindolymaleimide I	Calbiochem	Cat# 203290
Y27632	Calbiochem	Cat# 688000
LY294402	Calbiochem	Cat# 440204
U0216	Promega	Cat# V1121
ML141	Santa Cruz Biotechnology	Cat# 4266
C3 transferase	Cytoskeleton	Cat# CT04
GsMTx (Zebrafish)	TOCRIS	Cat# 4912
Blasticidin	Invitrogen	Cat# ant-bl
Zeocin	Invitrogen	Cat# ant-zn-5
G418 (Geneticin)	GIBCO	Cat# 10131027
Puromycin	Sigma-Aldrich	Cat# P8833
Tetracycline	Sigma-Aldrich	Cat# T7660
Doxycycline	Sigma-Aldrich	Cat# D3447
Trizol	Thermo Fisher	Cat# 15596026
Polyethylenimine “Max” MW 40,000	Polysciences, Inc.	Cat# 24,765
Type I collagen (Cellmatrix Type I-A)	Nitta Gelatin	N/A
Type I collagen (Cellmatrix Type I-P)	Nitta Gelatin	N/A
Hoechst 33,342	Life Technologies	Cat# H3570
Critical commercial assays		
CellTracker dye CMTPX	Life Technology	Cat# C34552
CellTracker dye CMFDA	Life Technology	Cat# C2925

(*Continued on next page*)

Continued

REAGENT or RESOURCE	SOURCE	IDENTIFIER
CellTracker dye CMAC	Life Technology	Cat# C2110
NucRed Live 647 ReadyProbe	Invitrogen	Cat# R37106
SiR-actin Kit	SPIROCHROME	Cat# CY-SC001
Flipper-TR	SPIROCHROME	Cat# SC020; Colom et al., 2016
MycoAlart	Lonza	Cat# LT07-118
Nucleofector 2b kit L	Lonza	Cat# VACA-1005
Lipofectamine 2000	Life Technology	Cat# 11668019
RNeasy Mini Kit	QIAGEN	Cat# 74,104
QuantiTect Reverse Transcription Kit	QIAGEN	Cat# 205311
GeneAce SYBR qPCR Mix	NIPPON GENE	Cat# 319-07683
STB-100 cell stretcher system	STREX	STB-100
STB-CH-04 stretch chamber	STREX	STB-CH-04
mMESSAGE mMACHINE SP6 Transcription Kit	Thermo Fisher	Cat# AM1340
Experimental models: Cell lines		
MDCK	Dr. W. Birchmeier	N/A
EpH4	Sigma-Aldrich	Cat# SCC284
Lenti-X^{TM} 293T cell Line	Takara	Cat# 632,180
Experimental models: Organisms/strains		
Zebrafish, wildtype (AB)	Dr. K. Kawakami	N/A
Zebrafish, Tg(krt4p:gal4; UAS:mKO2)	Dr. H. Wada	N/A
Zebrafish, Tg(krt4p:gal4; UAS:EGFP)	Dr. H. Wada	N/A
Oligonucleotides		
AHNAK2-shRNA forward: 5′-GATCCCCGCATATCG AGTGTCAATATTTCAAGAGAATATTGACACTCGAT ATGCTTTTTC-3′	This paper	N/A
AHNAK2-shRNA reverse: 5′-TCGAGAAAAAGCAAG TTCAAACTGCCAAATCTCTTGAATTTGGCAGTTTG AACTTGCGGG-3′	This paper	N/A
AHNAK2-sgRNA sequence: 5′-GTTCTCCAGGATG AGTCGTAGG-3′	This paper	N/A
Primer, AHNAK2 forward: 5′-GGGATGGACACCAG AAAGAA-3′	This paper	N/A
Primer, AHNAK2 reverse: 5′-GCGTGGACACTGTA ATGGTG-3′	This paper	N/A
Primer, β-actin forward: 5′-3 GGCACCCAGCAC AATGAAG-3	Takeuchi et al. (2020)	N/A
Primer, β-actin reverse: 5′-ACAGTGAGGCCAGG ATGGAG-3′	Takeuchi et al. (2020)	N/A
Recombinant DNA		
pCDH-EF1-Hygro-sgRNA vector	Kon et al. (2017)	N/A
pCDH-EF1-AHNAK2-sgRNA	This paper	N/A
pPB-TRE3G GFP	This paper	N/A
pPB-TRE3G GFP-RasV12	This paper	N/A
pPB-cmv-mCherry-Cdc42T17N	This paper	N/A
pPB-EF1-FLAG-AHNAK2-WT-IRES-Neo	This paper	N/A
pHR-EF1α-FLAG-AHNAK2-WT/-SA-cmv-Puro	This paper	N/A
pPB-EF1-MCS-IRES-Neo-GCaMP6s	Takeuchi et al. (2020)	N/A
pMD2G	Dr. Satoshi Toda	N/A
pCMV-dR8.2dvpr	Dr. Satoshi Toda	N/A
Plasmid: pT2 5xUAS-E1b-GAP43-EGFP-2A-RasV12	Haraoka et al. (2022)	N/A

(*Continued on next page*)

Continued

REAGENT or RESOURCE	SOURCE	IDENTIFIER
Plasmid: pT2 5xUAS-E1b-GAP43-EGFP-2A-stop	Haraoka et al. (2022)	N/A
Plasmid: pT2 5xUAS-E1b-GAP43-hmKO2-2A-H-RasV12	Takeuchi et al., 2020	N/A
Plasmid: pT2 5xUAS-E1b-GAP43-hmKO2-2A-stop	Dr. K. Kawakami	N/A
Plasmid: pCS2-GCaMP7	Dr. J. Nakai	N/A
Plasmid: pmtb-t7-alpha-bungarotoxin	Swinburne et al. (2015)	Addgene Plasmid#69542
Software and algorithms		
Metamorph	Molecular Devices	https://www.moleculardevices.co.jp/systems/metamorph-microscopy-automation-and-image-analysis-software
ImageJ	NHI Image	https://imagej.nih.gov/ij/download.html
GraphPad Prism 9	GraphPad Software	https://www.mdf-soft.com/products/prism9.html

RESOURCE AVAILABILITY

Lead contact

Further information and requests for resources and reagents should be directed to and will be fulfilled by the lead contact, Yasuyuki Fujita (fujita@monc.med.kyoto-u.ac.jp).

Materials availability

Plasmids or cell lines generated in this study will be made available on request, but we may require payment and/or a completed Materials Transfer Agreement if there is potential for commercial application.

Data and code availability

- Data reported in this paper will be shared by the lead contact upon request. The phospho-SILAC screening data generated during this study are available at https://molonc.researcherinfo.net/Phospho-SILAC screening.pdf.
- This paper does not report the original code.
- Any additional information required to reanalyze the data reported in this paper is available from the lead contact upon request.

EXPERIMENTAL MODEL AND SUBJECT DETAILS

Animals

Zebrafish wild-type strain (AB) and Tg [krt4:GAL4] line were raised and maintained under standard conditions and used at age 3-10 months. All experimental animal care was performed in accordance with institutional and national guidelines and regulations. The study protocol was approved by the Institutional Animal Care and Use Committee of Osaka University (RIMD Permit# R02-04).

Cell lines

MDCK, EpH4, HEK293, and Lenti-X 293T cells were used in this study. The parental MDCK cells were a gift from W. Birchmeier. EpH4 cells were purchased from Sigma-Aldrich. Lenti-X 293T cells were purchased from Takara. MDCK, EpH4, HEK293, and Lenti-X 293T cells were cultured in Dulbecco's modified Eagle's medium (DMEM) supplemented with 10% fetal bovine serum (FBS) (Sigma-Aldrich), 1% penicillin/streptomycin (Life Technologies), and 1% GlutaMax (Life Technologies) in a humidified 5% CO_2 incubator at 37°C. Mycoplasma contamination was regularly tested for all cell lines using MycoAlert Mycoplasma Detection kit (Lonza).

METHOD DETAILS

Antibodies, plasmids, and materials

The following antibodies were used in this study. Rabbit polyclonal affinity-purified anti-phospho-AHNAK2 antibody was generated using the following peptide as an antigen: FKMP[pS]FGAST (Medical & Biological Laboratories Co., Ltd.). Rabbit polyclonal affinity-purified anti-AHNAK2 antibody was generated using the following peptide as an antigen: KGHLPKVQMPSLKMPKVD (Cosmo Bio Co., Ltd.). Mouse anti-FLAG (M2) and mouse anti-filamin (F6682) antibodies were from Sigma-Aldrich. Mouse anti-β-actin (MAB1501R clone C4) antibody was from Merck Millipore. Mouse anti-GFP (#11814460001) antibody was from Roche. Rabbit anti-phospho-(Ser) PKC substrate (#2261) antibody was from Cell Signaling Technology. Mouse anti-Pan-Ras (Ab-3) antibody was from Calbiochem. Alexa-Fluor-568- and −647-conjugated phalloidin (Life Technologies) were used

at 1.0 U ml^{-1}. Alexa-Fluor-568-, −488-, and −647-conjugated secondary antibodies were from Life Technologies. Hoechst 33,342 (Life Technologies) was used at a dilution of 1:5,000. Amlodipine besylate (25 μM), SP600125 (10 μM), 18α-Glycyrrhetinic acid (αGA) (50 μM), Wiskostatin (25 μM), and Go6976 (10 μM) were from Sigma-Aldrich. GsMTx (10 μM) was from PEPTIDE INSTITUTE, Inc. Ionomycin (2 μM) was from FUJIFILM WAKO Pure Chemical Corporation. Bisindolylmaleimide (BIM)-I (10 μM), Y27632 (20 μM), and LY294002 (10 μM) were from Calbiochem. U0216 (10 μM) was from Promega. ML141 (20 μM) was from Santa Cruz Biotechnology. C3 transferase (1 μg/mL) was from Cytoskeleton. Type I-A collagen (Cellmatrix Type I-A) and Type I-P collagen (Cellmatrix Type I-P) were obtained from Nitta Gelatin and neutralized on ice to a final concentration of 2 mg mL^{-1} and 0.3 mg mL^{-1} according to the manufacturer's instructions, respectively. Type I-P collagen was used for traction force microscopy, whereas Type I-A collagen was used in the other experiments. NucRed Live 647 ReadyProbe was obtained from Invitrogen for the staining of cell nucleus for quantification of the nuclear aspect ratio. The Cell Tracker dyes CMFDA (green), CMTPX (red), and CMAC (blue) (Life Technologies) were used according to the manufacturer's instructions. The SiR-actin Kit (far-red silicon rhodamine (SiR)-actin fluorescence probe) for live imaging of F-actin and Flipper-TR (membrane tension sensor probe) were obtained from SPIROCHROME and used according to the manufacturer's instructions. Polyethylenimine "Max" MW 40,000 (PEI) was obtained from Polysciences, Inc.

Establishment of cell lines

MDCK cells stably expressing GFP (MDCK-pTR GFP), GFP-H-RasV12 (MDCK-pTR GFP-H-RasV12), or GFP-cSrcY527F (MDCK-pTR GFP-cSrcY527F) in a tetracycline-inducible manner were established and cultured as previously described (Hogan et al., 2009; Ohoka et al., 2015). MDCK-pTRE3G Myc-RasV12 cells were established and cultured as previously described (Kon et al., 2017). MDCK-GCaMP6s, MDCK-INF2-knockout (KO), and MDCK-GCaMP6s cells stably expressing TRPC1-shRNA (MDCK-GCaMP6s-pLKO-TetOn TRPC1-shRNA) or Piezo1-shRNA (MDCK-GCaMP6s-pLKO-TetOn Piezo1-shRNA) in a tetracycline-inducible manner were established and cultured as previously described (Takeuchi et al., 2020). To establish MDCK-pTRE3G Myc-RasV12-GCaMP6s cells, MDCK-pTRE3G Myc-RasV12 cells were transfected with PB-EF1-MCS-IRES-Neo-GCaMP6s by nucleofection (Nucleofector 2b Kit L, Lonza), followed by selection in the medium containing 800 μg mL^{-1} of G418 (Geneticin, Gibco). MDCK cells stably expressing AHNAK2-shRNA in a tetracycline-inducible manner were established as follows; AHNAK2-shRNA oligonucleotides (AHNAK2-shRNA: 5′-GATCCCCGCATATCGAGTGTCAATATTTCAAGAGAATATTGACACTCGATATGCTTTTTC-3′ and 5′-TCGAGAAAAAGCAAGTTCAAACTGCCAAATCTCTTGAATTTGGCAGTTTGAACTTGCGGG-3′) were cloned into the BglII/XhoI site of pSUPERIOR.*neo* + gfp (Oligoengine). MDCK cells were transfected with pSUPERIOR.*neo* + gfp AHNAK2-shRNA using Lipofectamine 2000 (Life Technologies), followed by selection in the medium containing 800 μg mL^{-1} G418. MDCK-pSUPERIOR.*neo* + gfp AHNAK2-shRNA cells were incubated with tetracycline for 72 h to induce sufficient knockdown prior to co-incubation with MDCK-pTRE3G Myc-RasV12 cells. To generate CRISPR/Cas9-mediated AHNAK2-knockout MDCK cells, the guide sequence of AHNAK2 single-guide RNA (sgRNA) targeting *Canis AHNAK2* was designed on exon 4, as described previously (Hsu et al., 2013; Kon et al., 2017). AHNAK2 sgRNA sequence (5′-GTTCTCCAGGATGAGTCGTAGG-3′) was introduced into the pCDH-EF1-Hygro-sgRNA vector. First, MDCK cells were infected with lentivirus carrying pCW-Cas9 and cultured in the medium containing 500 ng mL^{-1} of puromycin (Sigma-Aldrich). Tetracycline-inducible MDCK-Cas9 cells were pre-incubated with 2 μg mL^{-1} of tetracycline and transfected with pCDH-EF1-AHNAK2 sgRNA by nucleofection, followed by selection in the medium containing 200 μg mL^{-1} of hygromycin. Indels on the AHNAK2 exon in each monoclone were analyzed by direct sequencing using the following primers (5′-AAGCAGCAGGACCGAGAGT-3′ and 5′-TCTAGCACCTTCCACGCTTT-3′). To establish EpH4-GFP or EpH4-GFP-RasV12 cells, EpH4 cells were transfected with pPB-TRE3G GFP or pPB-TRE3G GFP-RasV12 by nucleofection (Nucleofector 2b Kit V, Lonza), followed by selection in the medium containing 10 μg mL^{-1} of Blasticidin (Invitrogen). To establish EpH4-GCaMP6s cells, EpH4 cells were transfected with PB-EF1-MCS-IRES-Neo-GCaMP6s by nucleofection (Nucleofector 2b Kit V, Lonza), followed by selection in the medium containing 800 μg mL^{-1} of G418 (Geneticin, Gibco). To establish MDCK-GCaMP6s-mCherry-Cdc42T17N cells, MDCK-GCaMP6s cells were transfected with pPB-cmv-mCherry-Cdc42T17N-EF1-Puro by nucleofection (Nucleofector 2b Kit L, Lonza), followed by selection in the medium containing 500 ng mL^{-1} of puromycin. AHNAK2 expression plasmids were constructed by the following, rather complex procedures, because the cDNA of the C-terminus of AHNAK2 was not obtained by PCR probably because it encompasses the six repeat domains that share extremely analogous DNA sequences. First, the cDNA encoding the N-terminus of canine AHNAK2 (amino acids 1-793 Uniprot: J9NZV9), which encompasses the first and second repeat domains, was amplified by PCR. For the generation of SA mutations in the PCR product, PrimeSTAR Max (Takara) was used according to the protocol in the PrimeSTAR(R) Mutagenesis Basal Kit. The rest of the C-terminus of AHNAK2 (amino acids 794-1648) was divided into five portions, and the corresponding oligonucleotides for canine AHNAK2-WT or AHNAK2-SA were synthesized using gBlocks(R) Gene Fragments (INTEGRATED DNA TECHNOLOGIES). The obtained cDNAs for the respective portions of AHNAK2 were sequentially cloned into pcDNA3-SVPuro-FLAG, so that FLAG tag was inserted at the N-terminal of AHNAK2. The AHNAK2 cDNA was then cloned into the NotI site of PB-EF1-MSC-IRES-Neo (PB533A). To establish MDCK-AHNAK2-KO cells stably expressing FLAG-AHNAK2-WT (MDCK-AHNAK2-KO + FLAG-AHNAK2-WT Rescue-2), MDCK-AHNAK2-KO cells were transfected with PB-EF1-FLAG-AHNAK2-WT-IRES-Neo by nucleofection (Nucleofector 2b Kit L, Lonza), followed by selection in the medium containing 800 μg mL^{-1} G418. To construct pHR-EF1α-FLAG-AHNAK2-WT-cmv-Puro or -SA-cmv-Puro, the cDNA encoding FLAG-AHNAK2-WT or -SA was cloned into the MluI/NotI site of pHR-EF1α vector (kindly provided by Dr. Satoshi Toda). To establish MDCK-AHNAK2-KO cells stably expressing FLAG-AHNAK2-WT or -SA (MDCK-AHNAK2-KO + FLAG-AHNAK2-WT Rescue-1, -SA Rescue-1, or -SA Rescue-2), MDCK-AHNAK2-KO cells were transfected with pHR-EF1α-FLAG-AHNAK2-WT-cmv-Puro

or -SA-cmv-Puro by the lentivirus infection, followed by selection in the medium containing 500 ng mL^{-1} of puromycin. For MDCK-pTRE3G Myc-RasV12, MDCK-pTRE3G Myc-RasV12-GCaMP6s, EpH4-pTRE3G GFP, or EpH4-pTRE3G GFP-RasV12 cells, 1 μg mL^{-1} of doxycycline (Sigma-Aldrich) was used to induce GFP or RasV12 expression. For tetracycline-inducible MDCK cell lines, 2 μg mL^{-1} of tetracycline (Sigma-Aldrich) was used to induce expression of proteins or shRNA.

Cell culture

For Figure S2A, HEK293 cells were transfected with PB-FLAG, PB-FLAG-AHNAK2-WT or -SA using Lipofectamine 3000 (Life Technologies) according to the manufacturer's instructions. At 24 h after the transfection, immunofluorescence analysis was performed. To examine the effect of inhibitors, except for the effect of GsMTx on apical extrusion, cells were incubated with the indicated inhibitor together with doxycycline or tetracycline for the indicated duration. For the analysis of the effect of GsMTx on apical extrusion, cells were incubated with GsMTx and tetracycline for 16 h, followed by wash out of GsMTx, and apical extrusion was analyzed at 24 h after the tetracycline addition. For production of lentivirus, Lenti-X 293T cells were cultured in a 6-well plate at approximately 80% confluence and transfected with pHR-EF1α-FLAG-AHNAK2-WT-cmv-Puro or -SA-cmv-Puro together with packaging plasmids (pMD2G and pCMV-dR8.2dvpr) using 2 mg mL^{-1} PEI. At 6 h after the transfection, the medium was changed, and cells were cultured for 42 h, followed by collection of the viral suspension. For the virus concentration, viral suspension was passed through a 0.45-μm filter (Corning), mixed with polyethylene glycol (PEG) solution (25.5% PEG +1.2 M NaCl), and precipitated by centrifugation (7,519 x g, 10 min, 4°C). MDCK-AHNAK2-KO cells were infected with lentivirus after incubation with 10 μg mL^{-1} polybrene (Sigma-Aldrich).

Phospho-SILAC (stable isotope labeling with amino acids in cell culture) screening

For SILAC labeling, cells were maintained in DMEM minus L-Lysine and L-Arginine (Cambridge Isotope Laboratories) supplemented with 10% dialyzed FBS and 1% penicillin/streptomycin (Gibco). Then, 50 μg mL^{-1} of U-^{13}C6-^{15}N2-L-lysine (Lys8) and 50 μg mL^{-1} of U-^{13}C6-^{15}N4 -L-arginine (Arg10) were added for "heavy" labeling, whereas 50 μg mL^{-1} of U-^{2}H4-L-lysine (Lys4) and 50 μg mL^{-1} of U-^{13}C6-L-arginine (Arg6) were added for "medium" labeling. In addition, 200 μg mL^{-1} of L-proline (Sigma-Aldrich) was added to the culture medium to prevent arginine to proline conversion. After two weeks of SILAC labeling, 1.0 x 10^7 heavy-labeled MDCK cells and 1.0 x 10^7 heavy-labeled MDCK-pTR GFP-RasV12 or MDCK-pTR GFP-cSrcY527F cells were mix-cultured in two 10-cm dishes. On the other hand, medium-labeled MDCK, MDCK-pTR GFP-RasV12, or MDCK-pTR GFP-cSrcY527F cells were separately cultured in a 10-cm dish. The SILAC labeled cells were cultured without tetracycline for 8-12 h, and then treated with 2 μg mL^{-1} tetracycline for 6 h or 10 h. The cell growth speed of normal, RasV12, or Src cells was not grossly affected by mix-culture, and the total cell numbers were eventually comparable between the heavy and medium SILAC culture conditions. Cells were then lysed in lysis buffer (50 mM Tris-HCl pH 8.5 and 1% sodium deoxycholate) followed by trichloroacetic acid precipitation. Protein concentration was measured using BCA protein assay kit (Pierce), and total 12 mg of protein lysate was prepared by combining different protein lysates (3 mg of medium-labeled normal or transformed cells cultured alone and 6 mg of heavy-labeled normal and transformed mix-cultured cells). The lysate mixture was reduced with 5 mM DTT at 55°C for 45 min, alkylated with 50 mM iodoacetamide at room temperature in the dark for 30 min, and further incubated with 2 μg mL^{-1} trypsin at 37°C for 16 h. After digestion, sodium deoxycholate was removed by ethyl acetate extraction (Masuda et al., 2008). Subsequently, peptides were submitted to fractionation and phosphopeptide enrichment. Peptide fractionation was performed by high pH reversed-phase chromatography (Wang et al., 2011). Briefly, tryptic peptides were loaded on XBridge C18 column (4.6 × 250 mm, 5 μm, Waters) and separated by gradient of acetonitrile (5–32% in 40 min) in 20 mM ammonium formate pH 10 at a flow rate of 1.0 mL min^{-1}. Peptides were collected every 30 s and then concatenated as described (Wang et al., 2011). Phosphopeptides from each fraction were enriched with titanium dioxide beads (Titansphere Phos-TiO kit, GL Science).

LC-MS/MS analysis

Peptide samples were analyzed with Q Exactive mass spectrometer coupled with the UltiMate 3000 nano-UHPLC system equipped with a trap column (PepMap C18, Thermo Fisher Scientific) and ESI tip column (75-μm i.d., 12-cm long, 3-μm C18 particles, Nikkyo Technos). Peptides were loaded to the trap column and subsequently eluted and separated using a linear gradient of 4–35% acetonitrile in 0.1% formic acid for 108 min with a flow rate of 300 nL min^{-1}. In the Q Exactive, full scan MS spectra were acquired in a range from m/z 350 to 1,600 at resolution 70,000, and the 10 most intense ions were sequentially fragmented in HCD (data dependent acquisition). Data analysis was performed using the Proteome Discoverer 2.2 software with the Mascot search engine. All MS/MS spectra were searched against the Uniprot dog proteome database (UP000002254), and peptide-spectrum matches (PSMs) were validated using Percolator at a 1% false discovery rate. For phosphopeptide analysis, the localization of phosphorylation site was validated by phosphoRS, and high confidence phosphopeptides (mascot score >40, PSM >15, and phosphoRS score 100) were selected for SILAC differential analysis. SILAC peptide quantification and calculation of the heavy/medium (mix-culture/mono-culture) ratio were performed with precursor ion quantifier node in Proteome Discoverer.

Immunofluorescence and western blotting

For immunofluorescence, MDCK, MDCK-AHNAK2-KO, MDCK-AHNAK2-KO + FLAG-AHNAK2-WT Rescue or -SA Rescue, MDCK-INF2-KO, MDCK-GCaMP6s, MDCK-GCaMP6s-pLKO-TetOn TRPC1-shRNA, or EpH4 cells were mix-cultured with MDCK-pTR GFP, MDCK-pTR GFP-RasV12, MDCK-pTR GFP-cSrcY527F, EpH4-pTRE3G GFP, or EpH4-pTRE3G GFP-RasV12 cells at a ratio

of 10:1 or 1:1 and plated onto collagen-coated coverslips as previously described (Hogan et al., 2009). The mixture of cells was incubated for 8-12 h, followed by tetracycline treatment for 6 h, except for analyses of apical extrusion, filamin accumulation, and the nuclear aspect ratio and cell height that were examined after 24 h, 16 h, and 10 h of tetracycline addition, respectively. Cells were fixed with 4% paraformaldehyde (PFA) in PBS and permeabilized, except that cells were fixed with methanol for the analysis of filamin accumulation as previously described (Kajita et al., 2014). Primary antibodies were used at 1:100, and all secondary antibodies were used at 1:200. Immunofluorescence images were analyzed with the Olympus FV1000 or FV1200 system using the Olympus FV10-ASW software. Images were quantified with the MetaMorph software (Molecular Devices) or the ImageJ software. For quantification of apical extrusion of RasV12-transformed cells, 50 xz-sections of immunofluorescence images of MDCK cells from ten randomly selected fields (212 μm × 212 μm) were analyzed for each condition. From these images, the ratio of apically extruded RasV12-transformed cells was calculated by the number of apically extruded GFP-positive cells relative to that of all GFP-positive cells. The frequency of perinuclear actin was calculated by the ratio of cells exhibiting perinuclear actin among cells mix-cultured with GFP-RasV12 cells. The analysis of filamin accumulation was performed as previously described (Kajita et al., 2014). For the quantification of the nuclear aspect ratio and cell height, 25 xz-sections of immunofluorescence images of MDCK cells from five randomly selected fields (141 μm × 141 μm) were analyzed for each condition. From these images with the staining of nucleus and F-actin, the nuclear aspect ratio (major axis/minor axis) and cell height were measured by the ImageJ software. Western blotting was performed as previously described (Hogan et al., 2004). Primary and secondary antibodies were used at 1:1,000. Western blotting data were analyzed using ImageQuant LAS4010 (GE healthcare).

Quantitative real-time PCR

MDCK-pSUPERIOR.*neo* + gfp AHNAK2-shRNA cells were cultured on 6-well plates (Corning). After incubation with tetracycline for 72 h, total RNA was extracted using Trizol (Thermo Fisher Scientific) and a RNeasy Mini Kit (QIAGEN) and reverse-transcribed using a QuantiTect Reverse Transcription Kit (QIAGEN). GeneAce SYBR qPCR Mix (NIPPON GENE) was used to perform qPCR using the StepOne system (Thermo Fisher Scientific). For data analysis, relative quantification analysis was performed using the comparative CT ($2^{-\Delta\Delta CT}$) method. For each sample, the mRNA level of AHNAK2 was normalized to the β-actin mRNA. The primer sequences were as follows. AHNAK2: 5′-GGGATGGACACCAGAAAGAA-3′ and 5′-GCGTGGACACTGTAATGGTG-3′; β-actin: 5′-GGCACCCAGCACAATGAAG-3′ and 5′-ACAGTGAGGCCAGGATGGAG-3′.

Time-lapse observation of cultured cells

For live-cell imaging, cells were incubated in Leibovitz's medium (L-15) (Gibco) containing 10% FBS. For the quantification of calcium sparks, MDCK-GCaMP6s, MDCK-GCaMP6s-TRPC1-shRNA, MDCK-GCaMP6s-Piezo1-shRNA, MDCK-GCaMP6s-mCherry-Cdc42T17N, or MDCK-pTRE3G Myc-RasV12-GCaMP6s cells were mix-cultured with MDCK or MDCK-pTRE3G Myc-RasV12 cells at a ratio of 10:1 or 1:1 and plated on the collagen-coated 35-mm glass bottom dish (Matsunami). The mixture of cells was incubated for 12-16 h until a monolayer was formed, followed by doxycycline treatment for 6 h. Then, they were observed with a 60× objective lens, capturing an image every 30 s for 4 h with Nikon confocal microscopy (A1 HD25). Time-lapse images at 6-10 h after induction of RasV12 expression were analyzed with the NIS-Elements software (Nikon) and the ImageJ software. For the quantification of the frequency of calcium sparks, the intensity of GCaMP was measured using the ImageJ software in 30 GCaMP-expressing cells surrounded by MDCK or RasV12 cells randomly selected from two fields in each experiment. The occurrence of calcium sparks was defined when the intensity of GCaMP surpassed the mean + 5SD (standard deviation). The value of 5SD was calculated from all of the analyzed GCaMP-expressing MDCK cells mix-cultured with MDCK cells in three experiments, whereas the mean value was from the analyzed cells in the respective experiment. For the quantification of calcium sparks in EpH4 cells, EpH4-GCaMP6s cells were mix-cultured with EpH4-pTRE3G GFP or EpH4-pTRE3G GFP-RasV12 cells pre-stained with CMTPX (red) at a ratio of 1:1 and observed by time-lapse imaging as described above. The GCaMP intensity was measured in EpH4-GCaMP6s cells directly contacting EpH4-GFP or EpH4-GFP-RasV12 cells. Calcium sparks were defined as described above, and the percentage of calcium spark-positive cells was quantified. For the analysis of cell movement, MDCK-GCaMP6s, MDCK-GCaMP6s TRPC1-shRNA, MDCK-INF2-KO, MDCK-AHNAK2-shRNA, MDCK-AHNAK2-KO, MDCK-AHNAK2-KO + FLAG-AHNAK2-WT Rescue, or -SA Rescue cells were mix-cultured with MDCK or MDCK-pTRE3G Myc-RasV12 cells at a ratio of 1:1 on the collagen-coated 35-mm glass bottom dishes. The former cells except MDCK-GCaMP6s and MDCK-GCaMP6s TRPC1-shRNA cells were pre-stained with CMFDA (green) before the mix-culture to distinguish from MDCK-pTRE3G Myc-RasV12 cells. At 6 h after the seeding, the mixture of cells was incubated in the medium containing the far-red silicon rhodamine (SiR)-actin fluorescence probes until the end of time-lapse imaging. At 24 h after the seeding, doxycycline was added, followed by time-lapse observation. To calculate the cell movement between 6 and 10 h after the doxycycline addition, the displacement of a centroid of normal or RasV12 cells was analyzed for each 1 h, and the sum of the displacement distances for 4 h was calculated.

For Figures 3D and 3E, MDCK-GCaMP6s cells mix-cultured with normal MDCK or MDCK-pTRE3G Myc-RasV12 cells were stained with far-red SiR-actin and Hoechst, followed by time-lapse imaging at 30-s intervals during 6–10 h after the doxycycline addition. Segmentation and tracking of each nucleus or cell in the captured images were performed using scikit-image (van der Walt et al., 2014). The fluorescence intensity of the GCaMP was converted to two-dimensional waveform data. Calcium sparks were defined as described above. The skimage regionprops tool was used to obtain the ratio of the major axis to the minor axis of a nucleus or cell. These data were also converted to waveform datasets, and the l1 trend filtering method was used to denoise (Kim et al.,

2009). The triangle threshold algorithm was applied to obtain the threshold for each morphological change (Zack et al., 1997). The points that were above or below the threshold value compared to the preceding frame were determined as the change points. The frequency of changes per frame was calculated in 50 frames before and after the calcium sparks. The frequency of changes without calcium sparks was calculated by dividing the number of changes throughout the entire period (6-10 h) by the total number of frames. A pairwise Wilcoxon sign sum test with Bonferroni correction ($p < 0.05$) was used to evaluate the difference between the frequency of changes with and without calcium sparks.

Stretching assay

Stretching assay was performed using the STB-100 cell stretcher system (STREX) for cells cultured on a flexible silicone membrane PDMS (polydimethylpolysiloxane) chamber (STB-CH-04, STREX) (20 mm × 20 mm) (Naruse et al., 1998). Before cell seeding, silicone membranes were coated with 5 μg mL^{-1} fibronectin (Sigma-Aldrich) at 37°C for 1 h. 8.0 x 10^5 MDCK cells were plated onto the silicone matrices in a neutral state in the device and grown to confluence. To stretch membranes with the STB-100 cell stretcher system device, one edge of the silicone membrane was clamped in place, while the other side was clamped to a movable shaft. The movable shaft was pulled out from 20 mm to 22 mm, resulting in stretch of 10% and kept for 60 min. Epithelial monolayers were fixed in 4% PFA/PBS at the stretched or neutral state, and after releasing silicone membranes from the stretcher system device, cells were analyzed by immunofluorescence.

Traction force microscopy and intracellular stress measurement

Traction force microscopy was performed using soft substrates. Such substrates were obtained by mixing the A and B parts of the silicone elastomer DOWSIL™ CY 52-276 with a ratio of 6:5 respectively to obtain a gel with a Young's modulus of 3 kPa (Kenry et al., 2015). The substrates were then coated with far-red beads (0.2 μm-diameter, Invitrogen F8807) to allow the tracking of cell displacements over time. The substrates were further coated with 0.3 mg mL^{-1} collagen at 4°C for 16 h and then washed with PBS. The mixture of MDCK-GCaMP6s cells and MDCK or MDCK-pTRE3G Myc-RasV12 cells was seeded on the substrate, followed by time-lapse imaging with a 25× objective lens, at 10-min intervals during 6–10 h after the doxycycline addition. After 10 h, 10% SDS was added to remove the cells, thus relieving the beads from the traction forces exerted by the cells; an image of the beads was then captured during the resting state of the gel. After stabilizing the movies to avoid drifting using the Image Stabilizer plug-in in ImageJ, the displacement of the beads was calculated using PIV (MatPIV) by comparing each frame of the acquired movie with the frame of the resting state of the beads (without cells). Interrogation windows of 96 pixels (around 16 μm) with overlap of 75% were used. The traction forces that the cells exert on their substrate were then calculated using the FTTC plugin (Tseng et al., 2012), knowing that the rigidity of the substrate used is 3 kPa and with a regularization factor of 8e-11 (Martiel et al., 2015). Finally, the intracellular stress inside the monolayer was calculated using the BISM MATLAB code (Nier et al., 2016). The isotropic stress that we used here was the average of the normal stress components of the stress tensor. For BISM analysis, the intracellular stress was calculated by hypothesizing that the cell height was constant within each monolayer. In the calculation, cell height values were not included, giving results in Pa.μm. To precisely obtain the stress results in Pa, we would need to divide them by the cell height value. As shown in Figure 3C, normal cells mix-cultured with RasV12 cells had a slightly increased height compared with normal cells cultured alone, meaning that were we to divide the stress values by the height of the cells, the difference between the isotropic stress would be more, not less (Figure 3F).

Membrane tension measurements by Flipper-TR

For membrane tension measurements, the fluorescent probe Flipper-TR was used. Cells were cultured on the collagen-coated 35-mm glass bottom dishes until the monolayer was formed. Cells were treated with 1 μM Flipper-TR at 37°C for 30 min to achieve appropriate labeling prior to imaging. The fluorescence lifetime of Flipper-TR was measured by FLIM (fluorescence lifetime imaging microscopy) using Leica SP8 FALCON confocal microscopy. Excitation was performed using a pulsed 514-nm laser operating at 40 MHz with emission collected through bandpass 585-795-nm filter gated with a HyD SMD detector. For the analysis of the Flipper-TR lifetime under hyper- or hypo-osmotic treatment, normal MDCK cells were cultured alone and, just prior to the analysis, incubated with the M199 medium (Gibco #11043023) containing 1% penicillin/streptomycin and 1% BSA (Sigma-Aldrich #2153). The lifetime of Flipper-TR in normal MDCK cells cultured alone was measured before and after the hyper-osmotic treatment (1 mL of M199 medium +1 mL of M199 medium containing 1.4 M sucrose) for 20 min or hypo-osmotic treatment (1 mL of M199 medium +2 mL of double distilled water) for 10 min. For Figure 3I, MDCK cells were mix-cultured with MDCK or MDCK-pTRE3G Myc-RasV12 cells pre-stained with CMAC (blue) at a ratio of 1:1. After making a monolayer, cells were incubated with L-15 medium containing 10% FBS and treated with doxycycline for 6 h, followed by Flipper-TR analysis. To examine the effect of ML141, the lifetime of Flipper-TR was analyzed after ML141 treatment for 30 min. For the quantification of Flipper-TR lifetime at cell-cell adhesions between normal cells (M-M) or between normal and RasV12 cells (M-R), the area of a cell-cell adhesion site was manually selected from the images showing plasma-membrane staining of Flipper-TR using ImageJ.

Zebrafish

One-cell stage embryos were used for injection. pCS2-GCaMP7 and pmtb-t7-alpha-bungarotoxin were used as templates for mRNA synthesis. mRNAs of GCaMP7 or bungarotoxin were synthesized using the SP6 mMessage mMachine System (Thermo Fisher

Scientific). To observe calcium sparks before apical extrusion of the outermost epithelial monolayer in zebrafish larvae, GCaMP7 mRNA (200 pg), pT2 UAS mKO2-T2A-RasV12 DNA (25 pg), and bungarotoxin mRNA (25 pg) were co-injected into the yolk of one-cell-stage embryos obtained by mating of the Tg [krt4:GAL4] line with wild-type zebrafish. Injected embryos were developed until 10-somite stage (14 hpf), treated with or without 2 μM GsMTx (TOCRIS) for 4 h. When injected embryos were developed until 18-somite stage (18 hpf), larvae carrying RasV12-transformed cells in the outermost epithelial monolayer were selected by confirming mosaic expression of mKO2 fluorescent proteins. Selected larvae were dechorionated and mounted in holes of a gel made with 1% low-melting point agarose (Nacalai Tesque) on 35-mm glass bottom dishes (Greiner Bio-One). Calcium sparks around mKO2-positive transformed cells were observed with a confocal microscope (FV3000, Olympus) by 2-h time-lapse imaging at 1-min intervals. In each time point of the time-lapse, z stack images of the larvae (ten planes at 100-200-μm intervals) were obtained. For control, pT2 UAS mKO2-T2A-stop DNA (15 pg) was co-injected with mRNAs of GCaMP7 and bungarotoxin. To analyze the cell movement and cell division before apical extrusion, pT2 UAS EGFP-T2A-RasV12 DNA (25 pg) and bungarotoxin were co-injected. After the injected embryos were developed until 2-cell stage, pT2 UAS GAP43-mKO2 DNA (25 pg) was injected into the cell body. The cell movement and cell division around EGFP-positive transformed cells were examined as described above except imaging at 10-min intervals. For control, pT2 UAS EGFP-T2A-stop DNA (15 pg) was co-injected with bungarotoxin. To analyze apical extrusion, pT2 UAS mKO2-T2A-RasV12 DNA (25 pg) was injected. GsMTx was washed out after 4 h incubation, and the injected embryos were developed until late somitogenesis stage (24 hpf). Apical extrusion of the mKO2-positive transformed cells was observed with a confocal microscope (FV3000, Olympus). Quantitative analysis of the calcium sparks and cell movement was performed using ImageJ/Fiji.

QUANTIFICATION AND STATISTICAL ANALYSIS

Statistical analysis

For data analyses, Chi-square test, paired or unpaired two-tailed Student's t-test, Wilcoxon signed rank test, one-way ANOVA with Dunnett's or Tukey's test, two-way ANOVA with Tukey's test, or Kruskal-Wallis test with Dunn's test was used to determine p values. p values less than 0.05 were considered to be statistically significant. No statistical method was used to predetermine sample size.